DETAIL.DOC

The Spectro-Radiometric Calibration Assembly (SRCA) of MODIS

(radiometric, spectral, and spatial calibrations)

Detailed support document to ATBD 1996

MCST Ref. No. MCM-SSATBD-01-U-R0C0

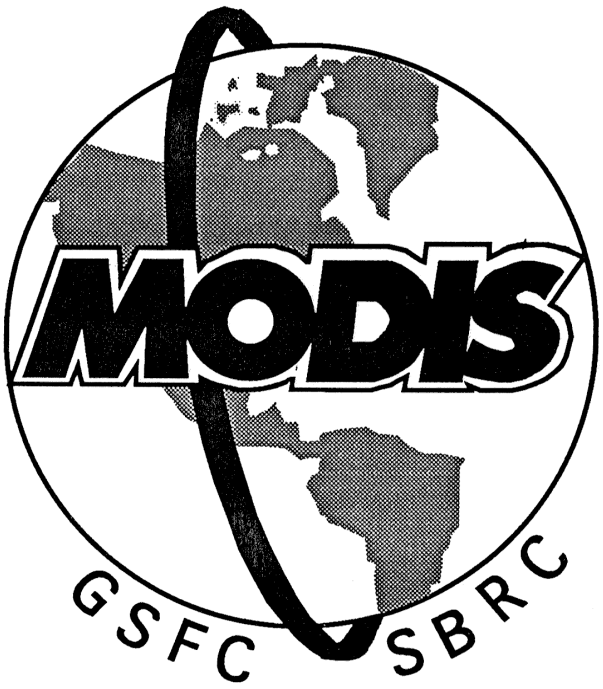

November 22, 1996
Revised April 25, 1997

Harry Montgomery /NASA
Nianzeng Che /Swales Aerospace

MODIS Characterization Support Team

Contents

1. Introduction

The Moderate Resolution Imaging Spectroradiometer (MODIS) instrument is one of five instruments for the Earth Observing System (EOS) platform scheduled to be launched in June 1998. The MODIS instrument takes spectral data over thirty- six bands covering visible(VIS), near infrared(NIR), short wave infrared (SWIR), middle wave infrared(MWIR), and long wave infrared (LWIR). The number of detectors varies from band to band. The land and cloud boundary bands, band 1(0.644 μm) and 2(0.855 μm), have forty detectors each with ground footprint of 0.25 km. The land and cloud property bands, bands 3(0.465 μm), 4(0.553 μm), 5(1.240 μm), 6(1.640 μm), and 7(2.130 μm), have twenty detectors each with ground footprint of 0.50 km. The rest of the twenty-nine bands for ocean color and atmosphere/cloud properties have ten detectors each with ground footprint of 1.00 km. Bands 13 and 14 have ten additional detectors each, designated bands 13hi and 14hi, for earth surface fire detection. The thirty-six bands are located on four focal plane assemblies(FPA): VIS, NIR, SWIR/MWIR, and LWIR.

MODIS radiometric uncertainty needs to be maintained to less than 5% throughout the MODIS life time (five years). However, the radiometric characteristics of heritage instruments indicate that the radiometric gain, count per $Wm^{-2}sr^{-1}\mu m^{-1}$, suffers from degradation on-orbit over time. Periodic calibration of MODIS on-orbit is imperative.

MODIS has four on-board calibrators (OBC): Blackbody(BB), Space View(SV), Solar Diffuser and Solar diffuser Stability Monitor (SD/SDSM), and Spectro-Radiometric Calibration Assembly (SRCA). The four OBCs are located such that they can be viewed sequentially by MODIS as the scan mirror rotates (Figure 1.1).

The BB and SV calibrate the thermal bands (Band 20-25, and 27-36) by providing a two-point calibration for each earth scan. An optional heated BB mode provides a temperature of 315K as a third calibration data point for detector non-linearity check.

The SD/SDSM and the SRCA calibrate the VIS and NIR bands (band 1-19 and 26). The SD/SDSM is expected to be a long-period stable calibrator for MODIS. The SDSM periodically measures the reflectance of the SD by forming the ratio of its signal when it views the SD and its signal when it views the sun for nine bands. Interpolation of the nine bands of data allows for calibrating the twenty MODIS bands. Constant correction of the SD reflectance using SDSM measurements enables radiance calibration during MODIS operation. Thus, radiometric gain change can be accurately tracked. For the EOS AM platform the radiometric calibration with the SD/SDSM occurs when the subsatellite point is near the north-pole and the earth and the atmosphere viewed by MODIS are in darkness.

The SRCA is not an absolute calibration source because it only partially fills the MODIS aperture (about 1/5 of the MODIS aperture area)(Figure 1.1). During the Activation and Evaluation (A&E) phase, the SRCA/MODIS system can carry the ground radiometric calibration onto orbit. This calibration will be transferred to the SD/SDSM. After A & E, the SRCA is not expected to be as good as the SD/SDSM. The SD/SDSM will maintain the radiometric calibration accuracy throughout the MODIS lifetime. In the MODIS operational phase, the SRCA can measure the calibration change intra-orbit and further provide radiometric calibration correction due to orbit-environment-related change.

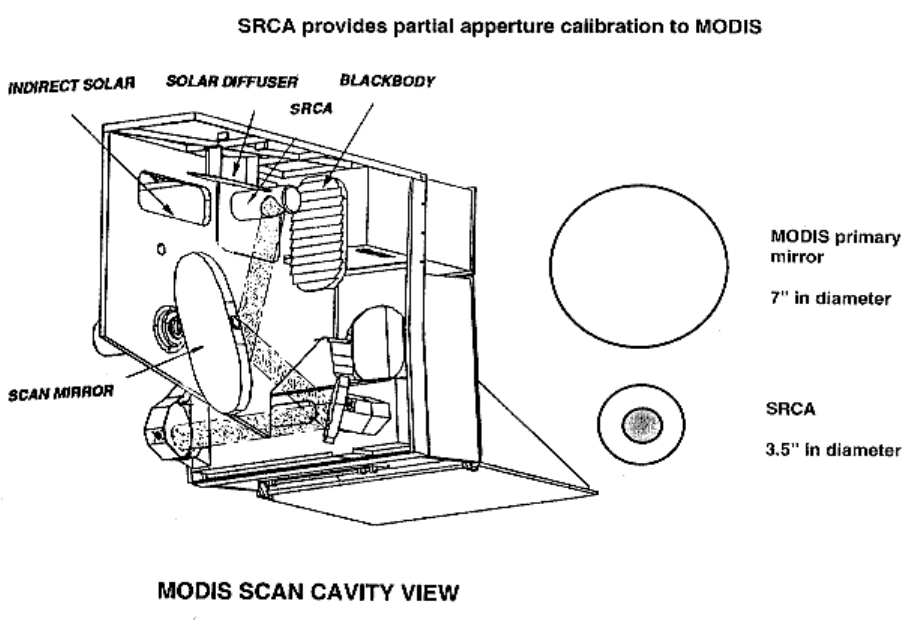

Figure 1.1 SRCA fills partial aperture of MODIS aperture

This document describes the detailed calibration algorithms using the SRCA. It is one of the detailed descriptions of a part of the MODIS level 1B calibration algorithms. The other two documents are: “Calibration of the MODIS emissive bands”, [MCST G003] by D. Knowles Jr., H. Montgomery, I. Goldberg, Nov. 16, 1995 and “MODIS solar reflective band calibration algorithm” [MCST G004] by R. Veiga, H. Montgomery, M. Jones, Dec. 15, 1996.

Covered in this document are the following sections: Instrument characterization, theoretical background of the algorithm, uncertainty analysis from data simulation, description of the algorithm, input data set requirement for the algorithms, and the algorithm products.

2. Instrument Characterization

The SRCA can be operated in any one of three calibration modes: radiometric, spectral, and spatial. The radiometric and spectral modes provide data only for band 1-19 and 26. The spatial mode provides data for all 36 spectral bands. The radiometric mode provides tracking of the radiometric calibration accuracy from prelaunch to on-orbit and tracking of the radiometric characteristics change intra-orbit. The MODIS band center wavelength shifts are periodically measured on-orbit when the SRCA is set in spectral mode. While in spatial mode the SRCA determines the detector position shifts along-scan and the band centroid shifts along-track. By combining the prelaunch Ground Support Equipment (GSE) detector location data, the prelaunch and on-orbit SRCA spatial mode data, and ground location for a nominal band provided by the MODIS Science Data Support Team (SDST), the ground geolocation can be determined.

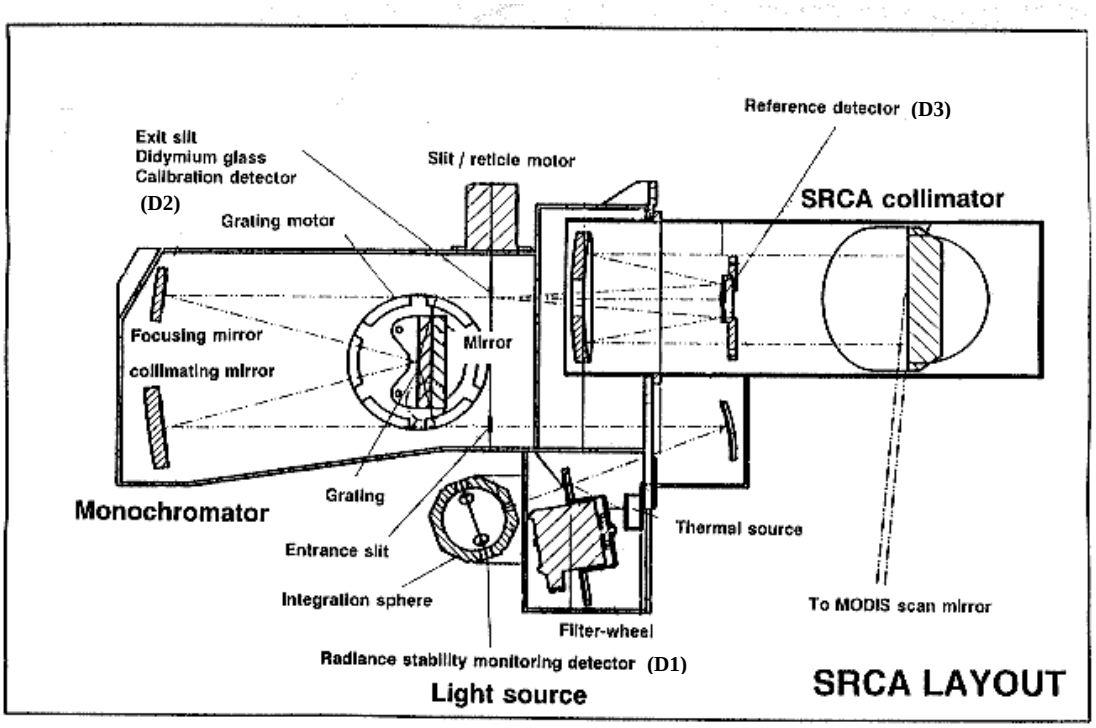

Figure 2.1 SRCA layout

The SRCA consists of three sub-assemblies: a light source, a monochromator/relay collimator, and a folded collimator (Figure 2.1).

The light source contains a Spherical Integrating Source (SIS), a thermal source, and a filter wheel. Six lamps (four 10W and two 1W) are embedded in the 2-inch diameter SIS. Four

of them are used to provide different output radiance levels and the other two lamps, one 10W and one 1W, are backups. This provides multi-level radiance to the MODIS bands for best operational signal level.

There are two temperature-controlled silicon photodiodes (SiPD), D1, embedded in the SIS. One is used as an alternate. The operational SiPD becomes active in constant radiance mode during A&E phase and in normal operation. The SiPD monitors the stability of the broadband radiance output from the SIS. When the SIS output changes, a feedback signal is generated and then amplified to adjust the lamp current until the SIS output returns to a preset constant value. The SRCA source control is switched to constant-current mode when one of the most frequently used lamps (one 10W or 1W) fails. Constant-current mode will then be used throughout the remainder of the MODIS lifetime.

The thermal resistance source is operated at 390K±5K in the spatial mode only, which provides radiation to the thermal bands.

The filter wheel located in front of the SRCA SIS can be placed at six positions: an open hole, a neutral density (ND) filter with transmittance of 0.25, three diffraction order sorting filters, or a dichroic beam-combiner. The dichroic beam-combiner transmits the light from the SIS and reflects the energy from the thermal source, providing spatial calibration for all MODIS bands.

The Czerny-Turner monochromator subassembly includes a slit/reticle section, a grating/plain mirror section, a collimating mirror, and a focusing mirror. The slit/reticle section is operated by a motor. There are three configurations controlled by the slit/reticle motor: (1) Entrance and exit slits in place; (2) Open hole (along-scan reticle) at the location of the entrance slit and the along-scan reticle in place at the focal plane of the focusing mirror, and (3) Open hole at the location of the entrance slit and the along-track reticle in place at the focal plane of the focusing mirror. When the exit slit is in position, a second exit slit, filtered with didymium glass, is operational (built in the same plate). The temperature-monitored calibration SiPD, D2, located behind the didymium glass provides the spectral calibration signal. The grating/plain mirror section is driven by a grating motor. Rotating the grating provides the spectral calibration. The radiometric mode and the spatial mode are provided with the plain mirror in place.

The folded collimator is a two-mirror Cassegrain telescope. A temperature-monitored reference SiPD, D3, with the same characteristics as the calibration SiPD, D2, is embedded at the center of the secondary mirror of the telescope, providing a reference signal for normalizing the calibration signal in the spectral mode. The reference SiPD signal will be saturated in the radiometric mode. The collimated beam is further reflected by a plain mirror and directed to MODIS.

The SRCA only partially fills the MODIS aperture. Thus, the collimated beam from the SRCA travels through a slightly different portion of MODIS compared to a beam filling the entire MODIS aperture. Corrections are required for compensation of the differences, which will be measured in a Thermal Vacuum chamber (TV) prelaunch.

3. The SRCA in radiometric mode

3.1 Physics of problem

The objectives of the SRCA radiometric mode are:
1) Track changes in MODIS reflective band (1-19 and 26) radiometric calibration from prelaunch to on-orbit.
2) Maintain the radiometric calibration accuracy on-orbit.
3) Track radiometric characteristics changes intra-orbit.

Different radiance levels are necessary for calibrating the MODIS bands at appropriate signal level. Six levels are available. The combination of 3-10W lamps and 1-1W lamp provides four light levels (3-10W, 2-10W, 1-10W, and 1-1W). Insertion of a neutral density (ND) filter for the 1-10W and 1-1W cases provides two additional light levels. The calibration begins with 3-10 W lamps turned on and the sequence, in general, is to turn-off lamps in order to reduce the warm-up time. That is 3-10W, 2-10W, 1-10W, 1-10W with ND, 1-1W, and 1-1W with ND. However, the 2-10W lamp configuration uses different lamps from the 1-10W lamp in order to minimize the use of the most frequently operated 1-10W lamp. For each MODIS band an optimum lamp configuration can be selected for radiometric calibration. Selection of the lamp configuration depends on the best Signal-to-Noise (SNR) ratio and digital counts (DN).

The SRCA is calibrated against the ground spherical integration source SIS(100) which is 100cm in diameter. SIS(100) is traced to the NIST standard with an uncertainty of 2.8%. Error in the transfer from the SIS(100) to the SRCA increases the uncertainty to 3.9% due to estimates of center wavelength shift, crosstalk, out-of-band response, polarization,

non-linearity, stray light, etc. Table 3.1.1 lists the error budget of MODIS radiometric calibration prelaunch.

The SRCA is expected to be a stable source. On orbit during the A&E phase , the SRCA will transfer the calibration to space by using the SRCA on-board SiPDs. The SiPD inside the SRCA SIS monitors and maintains the broadband radiance output stable while the reference SiPD in spectral mode tracks the launch-related spectral profile change of the SRCA output. These signals allow determination of the in-band radiances at the MODIS entrance pupil under the SRCA illumination during A&E. The radiometric calibration uncertainty is expected to be less than 3.9%. Before SRCA degradation it will transfer the calibration to the SD/SDSM one time with a radiometric uncertainty of 4.0%.

During operation, the SRCA radiometric accuracy decreases over time because of lamp degradation and changes in the coating reflectance of the SRCA SIS. In addition, the SRCA provides only partial aperture illumination to MODIS. The potentially transmissive variation over the MODIS aperture reduces the accuracy in radiance tracking. However, the SD/SDSM is expected to be invariant on orbit. After the SD/SDSM is calibrated against the SRCA during the A&E phase, the SD/SDSM becomes the reference source. The SRCA output will be periodically corrected on orbit using the SD/SDSM. By using the SD/SDSM, the SRCA is expected to be able to maintain radiometric uncertainty less than 4.4% on-orbit throughout the MODIS life-time (Table 3.1.2).

Table 3.1.1 Error budget of MODIS radiometric calibration prelaunch [5]

Uncertainty drivers	Radiance uncertainty (%)		
	Summary	Sub-summary	
SIS(100)	2.82		
(1) Irradiance/Radiance standard		0.50	
(2) Transfer to working standard		1.00	
(3) Standard lamp usage		1.69	
(3.1) Orientation			0.30
(3.2) Diffuser to lamp			0.50
(3.3) Current			0.50
(3.4) Linearity			0.50
(4) Halon diffuser		0.50	
(5) Monochromator		1.76	
(5.1) Scatter light			1.00
(5.2) Wavelength calibration			0.30
(5.3) Nonuniformity			1.00
(5.4) Geometric error			1.00
(6) SIS		0.71	

(6.1) Current control			0.50
(6.2) Nonuniformity			0.50
MODIS	2.28		
(1) SNR		0.50	
(2) Linearity		0.50	
(3) Crosstalk		0.50	
(4) Wavelength shift		1.00	
(5) Out-of-band response		1.24	
(6) Polarization		1.00	
(7) scatter		0.80	
(8) Stray light		0.50	
RSS Total	3.62		

Table 3.1.2 Uncertainty estimate of radiometric calibration using the SRCA

Item	Description	Uncertainty	
Requirement		5.0%	
(1) SRCA/MODIS transfers calibration into space		3.9%	
1	Calibration preflight at TV environment [Table 3.1.1]		3.6%
2	Transfer into space (1σ)		1.5%
(2) Transfer calibration from SRCA to SD/SDSM during A&E phase (1σ)		4.0%	
1	SRCA/MODIS transfers calibration into space		3.9%
2	Instability during radiometric calibration by SRCA		0.3%
3	Transfer from SRCA to SD/SDSM		1.0%
(3) SRCA radiometric uncertainty by referring to SD/SDSM in operation (1σ)		4.4%	
1	Transfer calibration from SRCA to SD/SDSM during A&E phase		4.0%
2	SD/SDSM uncertainty in space (TBD)		1.0%
3	Transfer from SD/SDSM to SRCA		1.0%
4	Instability during radiometric calibration by SRCA		0.3%
5	Instability between two radiometric calibration by SRCA		1.0%

3.2 Mathematical description of the algorithm

3.2.1 Determination of DN

The twenty reflective bands are located in three FPAs. During the radiometric mode, the along-scan reticle is in position. The reticle size, measured in 1-km IFOVs, is 5 IFOVs along-scan and 12 IFOVs along-track. The rectangular reticle is located at the focal plane of the focusing mirror in the monochromator (in place of the exit slit) so that the reticle is imaged onto the MODIS focal planes through the SRCA collimator and MODIS optical system. The reticle image scans across the detectors when the scan mirror rotates.

Figure 3.2.1 defines the DN value when MODIS detectors are fully illuminated by the SRCA under stable operational conditions.

The reticle image position under SRCA full illumination is determined by the detector response rather than a preset value according to the scan mirror angle because focal plane position shifts could affect the reticle positioning.

For a single mirror scan ten frames are available. The algorithm utilizes signal thresholds to count the starting and ending frame numbers and then picks up three out of four fully illuminated detector signals. The DNs are averaged over thirty-six scans of data and the detector/band signal stability is monitored.

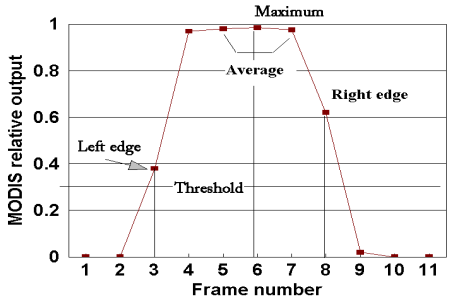

The effective DN (digital counts) should be used in all algorithms. For the effective DN the space DN has been subtracted and it has been further corrected for detector non-linearity, scan mirror reflectivity, temperature-related change, and scan angle effects.

Figure 3.2.1 Determination of DNs

The algorithm is as follows (Figure 3.2.1):

(1) Find the maximum DN, $DN_{max,b,ch}$, over all frames for a single scan.

(2) Set threshold

$$DN_{threshold}(scan\#) = 0.3 \cdot DN_{max,b,ch}(scan\#) \qquad (3.2.1.1)$$

(3) Determine the leftmost and rightmost frame numbers, F_{lf} and F_{rt}, for which the DNs are greater than $DN_{threshold}(scan\#)$.

(4) Find the middle frame number by averaging the leftmost and the rightmost frame numbers for each scan.

$$F_{mid} = Integer\left[\frac{F_{lf} + F_{rt}}{2}\right] \qquad (3.2.1.2)$$

(5) Average the three ***DN***s centered around the middle frame number for each scan and mirror side,

$$DN_{AV,b,ch}(scan\#) = \frac{1}{3}\sum_{F=F_{mid}-1}^{F=F_{mid}+1} DN_{b,ch}(F,scan\#) \qquad (3.2.1.3)$$

(6) Average ***DN***s over number of scans and number of mirror sides:

$$DN_{b,ch} = \frac{1}{N_{scan}}\sum_{1}^{N_{scan}} DN_{AV,b,ch}(scan\#) \qquad (3.2.1.4)$$

(7) Calculate the standard deviation over all scans.

3.2.2. Determination of lamp configuration utilized for each band

The implementation strategy for radiometric calibration is given in Table 3.2.1, where the lamp configuration is in turn-off order. The predicted ***DN*** values are listed in Table 3.2.2. The optimum lamp configuration is bolded in the table. The optimum values are the only ones used in the radiometric calibration. The optimum ***DN*** values are between 500 - 3000 counts for minimum quantization error and avoidance of saturation (80 percent of the maximum counts).

Two additional modes, 1-10W with ND and 1-1W with or without ND, are scheduled in the intra-orbit operation. The radiometric calibration for the two modes are: (1) 1-10W with ND for bands 2, 5, 6, 7, 10, 11, 12, 17, 18, 19, 26 and (2) 1-1W without ND for bands 5, 6, 7, 13, 14, 15, 17, 19, 26 and 1-1W with ND for band 16.

Table 3.2.1 Implementation strategy for radiometric calibration

No.	Source motor position	Grating motor position	Entrance & Exit slit motor	Lamp configuration	number of scans	MODIS band number
1	Open	Relay mirror	Along-scan reticle	3-10W	36	3, 8, 9
2	Open	Relay mirror	Along-scan reticle	2-10W	36	1, 4
3	Open	Relay mirror	Along-scan reticle	1-10W	36	10
4	ND filter	Relay mirror	Along-scan reticle	1-10W	36	2, 5-7, 11,12, 17-19,26
5	Open	Relay mirror	Along-scan reticle	1-1W	36	13-15
6	ND filter	Relay mirror	Along-scan reticle	1-1W	36	16

Table 3.2.2 Digital counts predicted using the SRCA in radiometric mode

			Lamp configuration					
MODIS Band	Center wavelength (μm)	Bandwidth (μm)	3-10W	2-10W	1-10W	1-10W w/ND	1-1W	1-1W w/ND
8	0.412	0.0142	**432**	288	144	41	2	1
9	0.442	0.0110	**1265**	843	422	118	9	2
3	0.466	0.0192	**417**	278	139	39	3	1
10	0.487	0.0106	3191	2127	**1064**	298	30	8
11	0.530	0.0120	satur.	satur.	2116	**593**	73	20
12	0.547	0.0106	satur.	satur.	3234	**906**	122	34
4	0.553	0.0197	1239	**826**	413	116	16	4
1	0.644	0.0499	1779	**1186**	593	166	32	8
13	0.665	0.0103	satur.	satur.	satur.	satur.	**801**	224
14	0.677	0.0116	satur.	satur.	satur.	satur.	**893**	250
15	0.746	0.0100	satur.	satur.	satur.	satur.	**1572**	440
2	0.855	0.0372	satur.	satur.	2484	**671**	218	59
16	0.866	0.0159	satur.	satur.	satur.	satur.	2522	**681**
17	0.904	0.0344	satur.	satur.	satur.	**1085**	380	103
18	0.935	0.0136	satur.	satur.	2956	**798**	293	79
19	0.935	0.0482	satur.	satur.	satur.	**1083**	400	108
5	1.240	0.0200	satur.	satur.	satur.	**1712**	865	234
26	1.375	0.0300	satur.	satur.	satur.	**1852**	1026	277
6	1.640	0.0246	satur.	satur.	satur.	**1720**	1081	292
7	2.130	0.0501	satur.	satur.	satur.	**1966**	1462	380
Notes: (1) The lamp configuration for radiometric calibration is where the DN is bolded.								
(2) Data from SBRS [25].								

3.2.3 Transfer radiometric calibration onto orbit

Radiometric calibration transfer from prelaunch to on-orbit depends upon the stability of both the MODIS and the SRCA output. During the A&E phase, MODIS radiometric characteristics are assumed to be unchanged and the SRCA will not be used for radiometric calibration transfer if:

(1) Both the signal changes of MODIS (illuminated by the SRCA in radiometric mode) and the SRCA SiPDs are less than 1.5% of their prelaunch values.

(2) Both signals change greater than 1.5% of their prelaunch values and the procedure introduced here shows that the changes are primarily attributable to the SRCA change.

Otherwise, this procedure will be executed. The science team will determine which bands shall have their radiometric gains adjusted. The uncertainty threshold of 1.5% change is considered reasonable for this procedure.

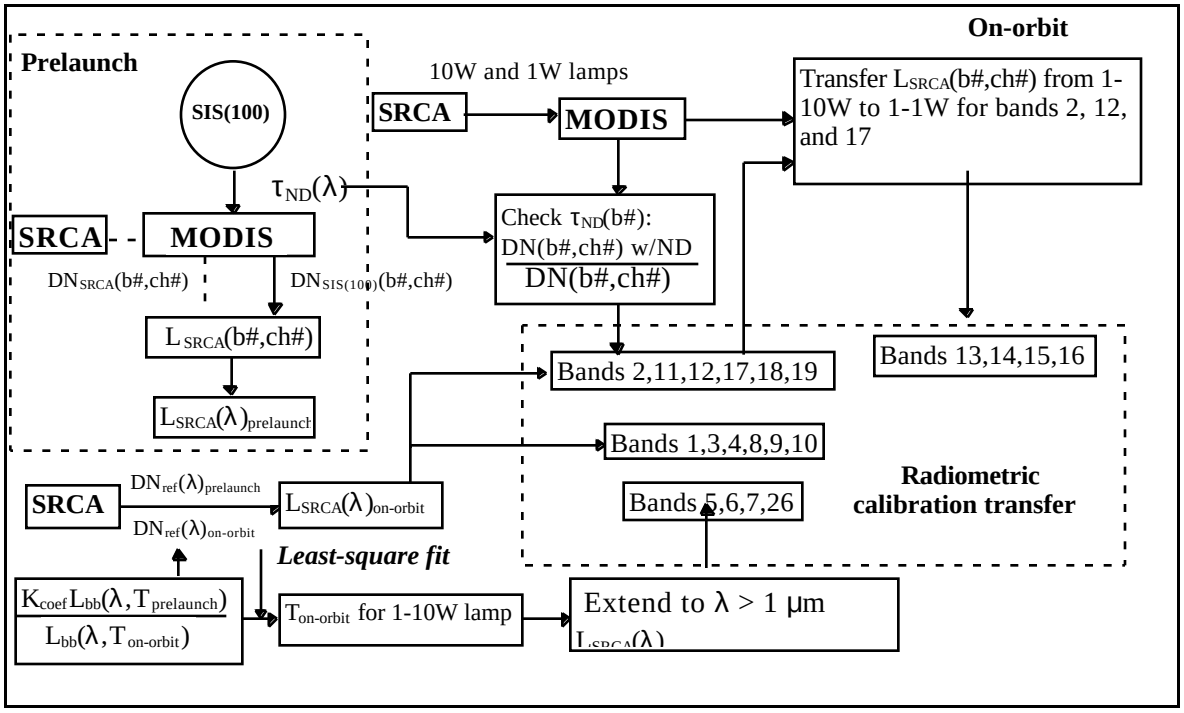

Figure 3.2.2 Flow chart of transfer radiometric calibration onto space

The SRCA is not used as an absolute calibration source because it only partially fills the MODIS aperture. But the SRCA is expected to be a stable transfer source. The radiometric calibration transfer utilizes the SRCA signals in spectral and radiometric modes both prelaunch and on-orbit along with the MODIS DNs.

The flow chart for transferring the radiometric calibration onto orbit is shown in Figure 3.2.2. The prelaunch signal processing is surrounded by the dashed-line box. The level 1B algorithm using on-orbit signals is shown outside the dashed-line box

3.2.3.1 Determination of $L_{SRCA}(\lambda)$ prelaunch

The SRCA is calibrated against the SIS(100) during TV testing. A detailed procedure is presented in Appendix A for converting SRCA in-band radiance to spectral radiance. For the lamp configurations of 1-10W and 3-10W bulbs, the in-band radiance is converted to a spectral radiance at a band center wavelength and spectral bandwidth which are computed from the spectral response of MODIS and the relative spectral output of the SRCA. The following model is derived in Appendix A:

$$L_{SRCA}(\lambda)_{prelaunch} = L_{SRCA}(\lambda, T) = q_{coef} \cdot A(\lambda) \cdot L_b(\lambda, T) \qquad (3.2.3.1)$$

This model is a least square fit to the SRCA data to generate a scale constant, q_{coef}, and lamp temperature, T, for lamp configurations of 1-10W and 3-10W. In this equation $L_b(\lambda, T)$ is the Planck function for computing black body radiance. The spectral radiance $L_{SRCA}(\lambda)_{prelaunch}$ provides the best estimate of the SRCA output in TV. Meanwhile, the reference SiPD signal, $DN_{ref,\,prelaunch}$, with dark reading subtracted in spectral mode is also collected.

3.2.3.2 Determination of $L_{SRCA}(\lambda)$ on-orbit

During the A&E phase, the MODIS DNs under the SRCA illumination are acquired. Meanwhile, the reference SiPD signal, $DN_{ref}(\lambda)_{on\text{-}orbit}$, is collected for lamp configuration with 3-10W and 1-10W in spectral mode. The spectral radiance of the SRCA on-orbit for each of the two lamp configurations is achieved by

$$L_{SRCA}(\lambda)_{on-orbit} = \frac{DN_{ref}(\lambda)_{on-orbit}}{DN_{ref}(\lambda)_{prelaunch}} \frac{(1+\Delta R_{SDS}(\lambda,T)\cdot(T_{H,prelaunch}-T_{H,o})}{(1+\Delta R_{SDS}(\lambda,T)\cdot(T_{H,on-orbit}-T_{H,o})} L_{SRCA}(\lambda)_{prelaunch} \quad (3.2.3.2)$$

Where $\Delta R_{SDS}(\lambda,T)$ is the response correction coefficient, T_H is the temperature of the SRCA housing, $T_{H,o}$ is the temperature at which the reference SiPD response is measured. Eq.(3.2.3.2) corrects for the temperature-related response variation due to SiPD temperature change. Notice that this equation contains data from both the radiometric mode and the spectral mode. Also the data used in this equation, acquired in the radiometric and spectral modes, must be with the same lamp configuration. Unfortunately, the lamp configuration with 2-10W are not planned for use in spectral calibration. The radiometric calibration transfer has to utilize the DN for 1-10W bands 1 and 4 (see Table3.2.2). If the radiances for the 1-10W lamp configuration for these two bands are known then the radiances for 2-10W will be calculated by multiplying those radiances by the DN ratio of 2-10W to 1-10W for those two bands.

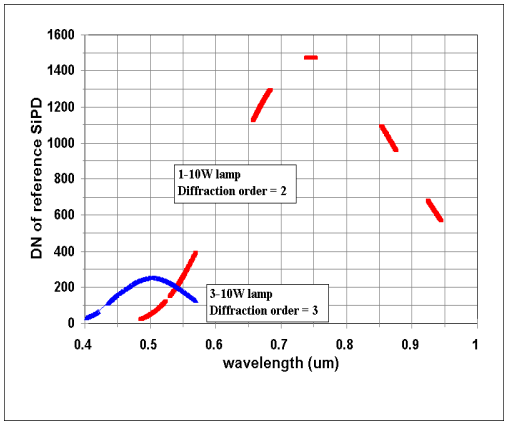

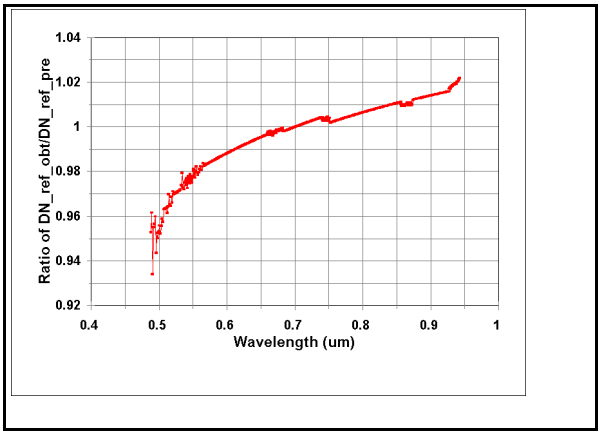

Figure 3.2.3 $DN_{ref}(\lambda)$ available for two lamp configurations

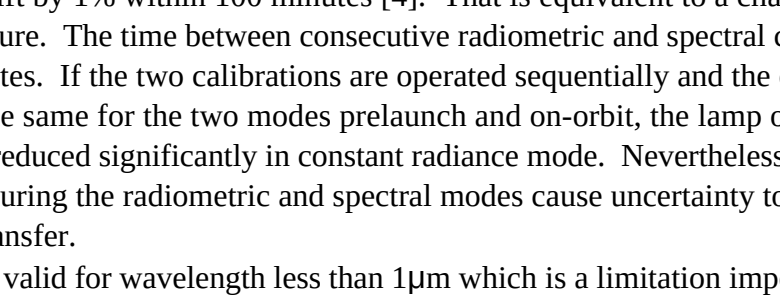

Figure 3.2.4. Ratio and values interpolation of $DN_{ref}(\lambda)_{on\text{-}orbit}$ /$DN_{ref}(\lambda)_{prelaunch}$

The operational environments for the spectral and radiometric modes differs significantly such as the polarization degree and the stray light level. However, using the ratio of the DNs measured in the same mode, prelaunch and on-orbit, minimizes these effects. The spectral output from the SRCA may vary on-orbit. It is estimated that the SRCA lamp output may drift by 1% within 100 minutes [4]. That is equivalent to a change of 4K in lamp temperature. The time between consecutive radiometric and spectral calibrations is about 80 minutes. If the two calibrations are operated sequentially and the order of operation is the same for the two modes prelaunch and on-orbit, the lamp output drift effect will be reduced significantly in constant radiance mode. Nevertheless, the spectral profile drifts during the radiometric and spectral modes cause uncertainty to the radiometric transfer.

Eq.(3.2.3.1) is valid for wavelength less than 1μm which is a limitation imposed by the reference SiPD response. The $\boldsymbol{DN_{ref}(\lambda)}$ as a function of λ is converted from digital counts of the reference SiPD as a function of grating motor angle, $\boldsymbol{DN_{ref}(\theta_m)}$, after the SRCA spectral calibration is executed for each lamp configuration. Figure 3.2.3 shows the $\boldsymbol{DN_{ref}(\lambda)}$ data utilized for the two lamp configurations (3-10W and 1-10W). The corresponding diffraction orders of the $\boldsymbol{DN_{ref}(\lambda)}$ curves for each MODIS band are marked on the figure and are listed in Table 3.2.3. In order to apply Eq.(3.2.3.2) the $\boldsymbol{DN_{ref}(\lambda)}$ and $\boldsymbol{L_{SRCA}(\lambda)_{prelaunch}}$ must be acquired for identical lamp configuration (i.e. both with 3-10W or 1-10W).

However, the data values available in the spectral calibration do not fully cover the bandwidths of the bands in Table 3.2.3. The spectral calibration for the 1-10W lamp configuration not only does not cover the entire band response for some required bands (11 and 2) but also misses data for bands 1 and 17.

Linear interpolation of the ratio values of the $\boldsymbol{DN_{ref}(\lambda)_{on\text{-}orbit} / DN_{ref}(\lambda)_{prelaunch}}$ (Figure 3.2.3) will provide the necessary data and the spectral radiance value on-orbit will be calculated by Eq.3.2.3.2. In Figure 3.2.4 the noisy-looking data is the available $\boldsymbol{DN_{ref}(\lambda)}$ (simulation) and the smooth-varying data points are the interpolated one. Limited lamp temperature change ensures that the interpolated values maintain their accuracy.

Table 3.2.3 The corresponding diffraction order and the lamp configuration of $DN_{ref}(\lambda)$ curve

Band	Wavelength (μm)	Lamp configuration of $DN_{ref}(\lambda)$ curve	Diffraction order for $DN_{ref}(\lambda)$ curve
8	0.412	3-10W	-3
9	0.442	3-10W	-3
3	0.466	3-10W	-3

10	0.487	1-10W	-2
11	0.530	1-10W	-2
12	0.547	1-10W	-2
4	0.553	1-10W	-2
1	0.644	1-10W	-2
2	0.866	1-10W	-2
17	0.904	1-10W	-2
18	0.935	1-10W	-2
19	0.935	1-10W	-2

3.2.3.3 In-band radiance, $L_{SRCA}(b\#)$

The in-band radiance for band 1, 3, 4, 8, 9, and 10 (as appropriate, 1-10 and 3-10W lamp configurations) is

$$L_{SRCA}(b\#) = \frac{\int_{\lambda_1(b\#)}^{\lambda_2(b\#)} L_{SRCA}(\lambda)_{on-orbit} R(\lambda) d\lambda}{\int_{\lambda_1(b\#)}^{\lambda_2(b\#)} R(\lambda) d\lambda} \quad (3.2.3.3)$$

and the in-band radiance for band 2, 11, 12, 17, 18, 19 (10W with ND) is

$$L_{SRCA}(b\#) = \frac{\int_{\lambda_1(b\#)}^{\lambda_2(b\#)} \tau_{ND}(\lambda) L_{SRCA}(\lambda)_{on-orbit} R(\lambda) d\lambda}{\int_{\lambda_1(b\#)}^{\lambda_2(b\#)} R(\lambda) d\lambda} \quad (3.2.3.4)$$

where $\tau_{ND}(\lambda)$ is the spectral transmittance of the ND filter. The values of $\tau_{ND}(\lambda)$ are measured prelaunch and the spectral profile can be assumed to be unchanged on-orbit. Check of the variation of $\tau_{ND}(\lambda)$ on-orbit is introduced in 3.2.3.4. The integration is over the band response.

3.2.3.4 Check of ND filter transmittance on orbit

The ND filter transmittance is not expected to change from prelaunch to on-orbit. The prelaunch transmittance value can be utilized on-orbit. However, check of the ND filter transmittance on-orbit is straight forward and the ND filter transmittance deduced on-orbit may provide useful information about the stability of the characteristics of the ND filter.

Figure 3.2.5 illustrates the spectral transmittance of the ND filter measured by SBRS.

Check of the ND filter transmittance is feasible on-orbit by computing the ratio of DNs for band 5, 6, 7, 10, and 15 because proper DN values with and without ND filter are available for the five bands. That is

$$\tau_{ND}(b\#)_{orbit} = \frac{1}{N_{ch}(b\#)} \sum_{1}^{N_{ch}(b\#)} \frac{DN_{SRCA,10W}(b\#,ch\#) \quad withND}{DN_{SRCA,10W}(b\#,ch\#)} \tag{3.2.3.5}$$

We calculate the in-band transmittance for the on-orbit case using

$$\tau_{ND}(b\#)_{calculated} = \int_{\lambda'_1(b\#)}^{\lambda'_2(b\#)} \tau_{ND}(\lambda) d\lambda \tag{3.2.3.6}$$

where the cut-in and cut-off wavelengths, $\lambda'_1(b\#)$ and $\lambda'_2(b\#)$, are obtained from spectral calibration on-orbit. The spectral profile of the ND filter transmittance is assumed to be unchanged.

An adjustment coefficient, A_{ND}, is introduced which averages the ratios of the five $\tau_{ND}(b\#)_{on\text{-}orbit}$ to the calculated values, $\tau_{ND}(b\#)_{calculated}$.

$$A_{ND} = \frac{1}{5} \sum_{1}^{5} \frac{\tau_{ND}(b\#)_{on-orbit}}{\tau_{ND}(b\#)_{calculated}} \tag{3.2.3.7}$$

The spectral transmittance of the ND filter on-orbit is

$$\tau_{ND}(\lambda) = A_{ND} \cdot \tau_{ND}(\lambda)_{prelaunch} \tag{3.2.3.8}$$

A warning flag will be set if the ND filter transmittance changes greater than 1% by calculation. The science team will make the decision whether to use the prelaunch values of $\tau_{ND}(b\#)_{prelaunch}$ or to apply the newly predicted values of τ_{ND} in Eq.(3.2.3.8).

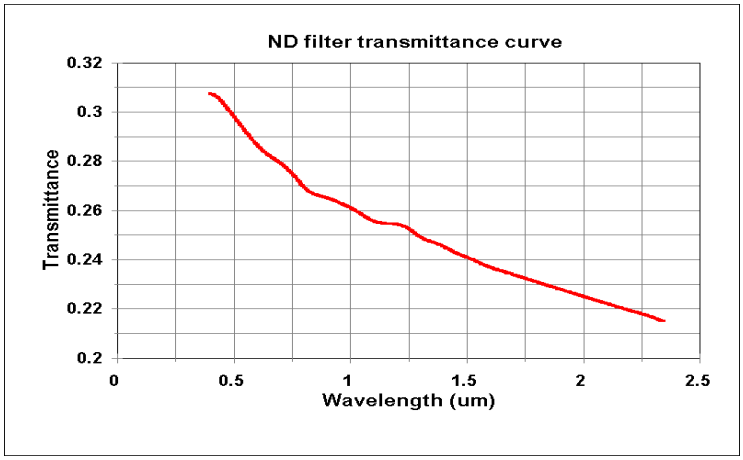

Figure 3.2.5 Spectral transmittance of the ND filter

3.2.3.5 Determination of spectral radiance change for λ > 1μm

To determine the unknown values of $L_{SRCA}(b\#)$ for wavelength greater than 1μm (bands 5, 6, 7, and 26) the band ratios between these bands and a reference band is computed. Then by multiplying the four ratios by the known band radiance with λ < 1 μm we determine the band radiances for λ > 1 μm. The on-orbit SRCA SIS radiometric temperature is required to compute the ratio. A least-square fit is applied to predict the radiometric temperature change for 1-10W lamp on-orbit. We assume that the $L_{SRCA}(\lambda)$ profile change is attributed only to the lamp temperature change on-orbit. Using the reference SiPD spectral signals (more than 200 data points) for λ < 1 μm, the two unknowns, curve adjusting coefficient, q_{coef}, and the 1-10W lamp temperature, $T_{on\text{-}orbit}$, are determined by fitting

$$\frac{DN_{ref}(\lambda)_{on-orbit}}{DN_{ref}(\lambda)_{prelaunch}} = q_{coef}\frac{L_b(\lambda, T_{on-orbit})}{L_b(\lambda, T_{prelaunch})} \qquad (3.2.3.9)$$

where $T_{prelaunch}$ is from Appendix A, q_{coef} is a constant and $L_b(\lambda,T)$ is calculated by Planck's equation.

Assume that for the spectral mode the i-th data point ***DN*** values for the reference SiPD, prelaunch and on-orbit, are known. The ratio of the two DNs is:

$$R_{f,i} = \frac{DN_{ref}(\lambda_i)_{on-orbit}}{DN_{ref}(\lambda_i)_{prelaunch}} \qquad (3.2.3.10)$$

Set

$$R_{t,i}(q_{coef}, T_{on-orbit}) = q_{coef} \cdot \frac{exp(14388/\lambda_i / T_{prelaunch} - 1)}{exp(14388/\lambda_i / T_{on-orbit} - 1)} \qquad (3.2.3.11)$$

where $T_{prelaunch}$ is the radiometric temperature of the lamp in the SRCA SIS. The method of deduction of the lamp temperature is detailed in Appendix B.

The difference $R_{ss,i} = R_{t,i}(q_{coef}, T_{on-orbit}) - R_{f,i}$ (3.2.3.12)

The first derivatives of the $R_{t,i}(q_{coef}, T_{on-orbit})$ are

$$ds_{coef,i} = \frac{\partial R_{t,i}(q_{coef}, T_{on-orbit})}{\partial q_{coef}} = \frac{exp(14388/\lambda_i / T_{prelaunch} - 1)}{exp(14388/\lambda_i / T_{on-orbit} - 1)} \qquad (3.2.3.13)$$

$$ds_{T,i} = \frac{\partial R_{t,i}(q_{coef}, T_{on-orbit})}{\partial T_{on-orbit}} = \frac{14388\, q_{coef}}{\lambda_i T_{on-orbit}^2} \cdot ds_{coef,i} \qquad (3.2.3.14)$$

Calculation of matrix coefficients and the procedure of the least-square fit are described in Appendix A. The initial temperature for the looping starts with a nominal lamp temperature.

Extrapolation of radiance from $\lambda < 1$ μm to $\lambda > 1$ μm is feasible because the spectral radiance change due to filament temperature variation is less sensitive for long wavelength than for short wavelength.

3.2.3.6 Determination of the in-band radiance for $\lambda > 1$μm

The use of a least-square fit to predict the lamp temperature for 1-10W lamp provides the best estimate of spectral radiance shape change over the wavelength range of interest. However, it is proper to use the spectral shape of the SRCA ouput on-orbit rather than the spectral radiance values. We set the relative spectral radiance as (See Appendix A)

$$l_{SRCA}(\lambda) = A(\lambda) L_b(\lambda, T_{on-orbit}) \qquad (3.2.3.15)$$

The in-band radiance ratio for band 5, 6, 7, and 26 to a reference band can be evaluated from the $l_{SRCA}(\lambda)$ curve. Anchoring the ratio to the in-band radiance for the reference band gives the in-band radiance for band 5, 6, 7, and 26. That is

$$L_{SRCA}(b\#) = \frac{\int_{\Delta\lambda(b\#)} l_{SRCA}(\lambda)d\lambda}{\int_{\Delta\lambda(b\#)} d\lambda} \cdot \frac{\int_{\Delta\lambda(bo\#)} d\lambda}{\int_{\Delta\lambda(bo\#)} l_{SRCA}(\lambda)d\lambda} \cdot L_{SRCA}(bo\#) \qquad (3.2.3.16)$$

where ***b#*** is the band number for which the radiance is to be determined and ***b0#*** is the reference band number, band 17, with radiance known. Although the spectral radiance for band 17 is not available directly from the ratio of $DN_{ref}(\lambda)_{on\text{-}orbit} / DN_{ref}(\lambda)_{on\text{-}orbit}$ for 1-10Wbut from interpolation, the band 17 (0.904μm) is less sensitive to the lamp temperature change.

3.2.3.7 Transfer radiances from 10W to 1W lamp configuration

Transfer in-band radiances from 1-10W with ND to 1-1W uses DN ratios for bands 12, 2, and 17.

The band radiance for 1-1W lamp is calculated by the MODIS detector DN ratio multipled by the band radiance for the 10W lamp with ND

$$L_{SRCA}(b\#,1W) = L_{SRCA}(b\#,10W) \cdot \tau_{ND}(b\#) \bullet \frac{DN_{SRCA}(b\#,ch\#,1W)}{DN_{SRCA}(b\#,ch\#,10W)} \quad (3.2.3.17)$$

In this equation $DN_{SRCA}(b\#,ch\#,10W)$ is with the ND in place.

3.2.3.8 Interpolation to determine the band radiance for bands 13-16

Now we know the band radiances for bands 12, 2, and 17. The center wavelengths of bands 13(0.665μm), 14(0.677μm), and 15(0.746μm) are sandwitched by bands 12(0.547μm) and 2 (0.855μm) and band 16 (0.866μm) by bands 2(0.855μm) and 17(0.904μm). The relative spectral curve of the SRCA output for 1W lamp measured prelaunch is utilized to determine the band ratios of the TBD bands, ***b#,*** to the anchoring bands, ***b1#*** and ***b2#.*** The in-band radiances for the four TBD bands are the average from the two independent anchoring radiances.

$$L_{SRCA}(b\#) = \frac{1}{2}\left[\frac{\int_{\Delta\lambda(b\#)} l_{SRCA}(\lambda)d\lambda}{\int_{\Delta\lambda(b\#)} d\lambda} \cdot \frac{\int_{\Delta\lambda(b1\#)} d\lambda}{\int_{\Delta\lambda(b1\#)} l_{SRCA}(\lambda)d\lambda} \cdot L_{SRCA}(b1\#)\right] + \frac{1}{2}\left[\frac{\int_{\Delta\lambda(b\#)} l_{SRCA}(\lambda)d\lambda}{\int_{\Delta\lambda(b\#)} d\lambda} \cdot \frac{\int_{\Delta\lambda(b2\#)} d\lambda}{\int_{\Delta\lambda(b2\#)} l_{SRCA}(\lambda)d\lambda} \cdot L_{SRCA}(b2\#)\right] \quad (3.2.3.18)$$

Anchoring band radiances to two neighbor bands significantly reduces the effect of the 1W lamp tempelature variation on the radiance deduction on-orbit.

3.2.3.9 Using flat-fielding information to correct the SRCA non-uniformity effect

The MODIS detectors in the focal plane are expected to be non-uniformly illuminated by the SRCA. The entrance slit illuminated by the SRCA SIS may be non-uniform because the SIS source is a sphere instead of a flat extended source. The aberration of the SRCA optical system will contribute to the non-uniform illumination of the MODIS detector focal plane. The radiometric calibration transfer discussed above tracks the average radiance change. However, the radiance value that may vary from detector to detector.

The solar diffuser is an excellent uniform and Lambertion surface. Under the illumination of the sun, a uniform illuminating field will be achievable. This provides a source for relative radiometric calibration between detectors and possible correction for the non-uniformity effect of the SRCA.

The MODIS detector DN under the illumination of SD can be simply expressed as

$$DN_{SD}(b\#, ch\#) = G(b\#, ch\#) \cdot L_{SD}(b\#) \quad (3.2.3.19)$$

where G is the radiance gain of the detector and L_{SD} is the radiance of the SD.

When the SRCA is illuminating the MODIS detectors, a similar expression can be written as

$$DN_{SRCA}(b\#, ch\#) = G(b\#, ch\#) \cdot L_{SRCA}(b\#) \cdot C_{SRCA}(b\#, ch\#) \quad (3.2.3.20)$$

where C_{SRCA} is the correction coefficient for non-uniform illumination.

We ignore the vignetting of the reticle because the MODIS detector is located one IFOV (1 km) away from the reticle edges in along-track direction. Also we do not consider the non-uniformity along-scan because the reticle scans across the detector. The average value of C_{SRCA} is normalized to one over the detectors of a band without compromising accuracy.

$$\frac{1}{N_{ch}} \sum_{ch=1}^{N_{ch}} C_{SRCA}(b\#, ch\#) = 1 \qquad (3.2.3.21)$$

Combining Eqs.(3.2.19)-(3.2.3.21), we have

$$C_{SRCA}(b\#, ch\#) = \frac{N_{ch}}{\sum_{ch=1}^{N_{ch}} \frac{DN_{SRCA}(b\#, ch\#)}{DN_{SD}(b\#, ch\#)}} \cdot \frac{DN_{SRCA}(b\#, ch\#)}{DN_{SD}(b\#, ch\#)} \qquad (3.2.3.22)$$

The radiance of the SRCA for detector number ***ch#*** of a band ***b#*** is

$$L_{SRCA}(b\#, ch\#) = L_{SRCA}(b\#) \cdot C_{SRCA}(b\#, ch\#) \qquad (3.2.3.23)$$

3.2.4 Radiance gain

The radiance gain is calculated by

$$G(b\#, ch\#) = \frac{DN_{SRCA}(b\#, ch\#)}{L_{SRCA}(b\#, ch\#)} \qquad (3.2.4.1)$$

The $L_{SRCA}(b\#,ch\#)$ is obtained on-orbit by:

1) Using prelaunch values during the first two months and continuing to use them during the A&E phase if on-orbit data indicate the prelaunch values have not changed.

(2) Implementing the algorithm introduced above if the MODIS science team agrees that the radiance gain has changed and the adjustment is needed.

(3) Using SD/SDSM calibration in operation after the A&E phase.

3.3 Uncertainty estimates

Various uncertainties are expected when transferring from prelaunch to on-orbit using the SRCA/MODIS system. Figure 3.3.1 shows estimated uncertainties for SRCA transfer of radiometric calibration onto orbit. The results are from a Monte-Carlo simulation. Table 3.3.2 lists the uncertainty components and their ranges. A typical case is given for band 8.

Table 3.3.2 Radiance uncertainty for carrying the radiometric calibration onto space

Item	Description	uncertainty	Band 8 case (%)
1	Quantization uncertainties of the SRCA and MODIS signal	1/DN/ √ No. averaged	negligible
2	Convert from band to center wavelength	Determined by the algorithm	0.03
3	SRCA SIS constant radiance control	< 0.05%	0.05
4	Reference SiPD temperature measurement	2 K	0.19
5	Reference SiPD quantization and SNR	1/SNR/ √ No. averaged	0.40
6	Stray-light	3%	0.10
7	Uncertainty in center wavelength	Band shift by 0.5 - 0.7 nm (1)	0.52
8	Uncertainty in wavelength scale on radiance determination	$d\beta$ and $d\theta_{off}$ (1)	0.32
9	slit width effect on determination of spectral radiance		0.15
10	Uncertainty in transfer coefficients, c(b#)	Color Temperature. change 20K	negligible
11	Non-uniformity correction	Simplified STOP results	0.17
12	Mirror reflectivity (2)	no change	--
13	Uncertainty in lamp temperature prediction	10K	--
	Total		0.80

(1) From spectral calibration results (2) PL3095-Q04995, SBRC, 5/95

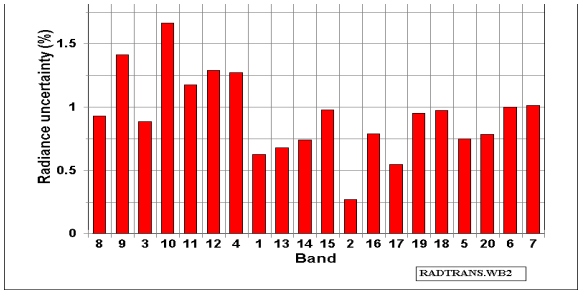

Figure 3.3.1 Radiance uncertainty for radiometric calibration transfer onto orbit

3.4 Description of input data set, output products, and quality control

3.4.1 Input data set:

(1) The SIS(100) in-band radiance for each MODIS band measured in TV, $L_{SIS(100)}(lamp,b\#)$.

(2) The spectral radiance of SIS(100) during the SRCA radiometric calibration in TV, $L_{SIS(100)}(lamp,\lambda)$.

(3) The spectral transmittance of the ND filter, $\tau_{ND}(\lambda)$.

(4) The spectral signal (***DN***) of the reference SiPD in terms of wavelength $DN_{ref}(\lambda)_{prelaunch}$ and $DN_{ref}(\lambda)_{on\text{-}orbit}$.

(5) Spectral response of the reference SiPD, $R(\lambda)$, measured at T_o.

(6) The temperature coefficient of the reference SiPD in terms of wavelength and temperature, $\Delta R(\lambda,T)$.

(7) The SRCA wavelength self-calibration results (center wavelength and shift for MODIS bands, and monochromator parameters) measured prelaunch and on-orbit, $\lambda_c(b\#,ch\#)$, $\Delta\lambda_c(b\#,ch\#)$, $\beta(lamp)$, and $\theta_{off}(lamp)$.

(8) The spectral responses of the MODIS bands measured prelaunch in TV, $R(b\#,\lambda)$.

(9) The SRCA spectral radiance output profiles for 10W and 1W lamps measured at sub-assembly level, $l_{SRCA}(\lambda)$.

3.4.2 Output products:

(1) Prelaunch: Radiance calibrated against the SIS(100) for SRCA full radiometric calibration, $L_{SRCA}(b\#,ch\#)$.

(2) Transfer reflective band radiometric calibration on-orbit: Radiance for SRCA full radiometric calibration mode during the A&E phase, $L_{SRCA}(b\#,ch\#)$.

(3) Intra-orbit radiometric calibration: Radiance for:

- SRCA in full radiometric calibration.
- SRCA 10W radiometric calibration continuous over cycles of orbit.
- SRCA 1W with and without ND filter radiometric calibration continuous over cycles of orbit.

Off-line product:

Trending of MODIS calibration using the SRCA.

3.4.3 Data report format

Each radiance value reported should be tagged with:

- Date and time
- SRCA lamp configuration
- ND filter: clear or in position
- SRCA source controller: primary or redundant
- SRCA source control mode: constant radiance or constant current
- Standard deviation of DNs for the active bands.

3.4.4 Quality control and diagnostics

(1) Before the radiometric calibration is applied, a step-by-step diagnostic procedure will be executed to assess MODIS and the SRCA normality on-orbit.

(2) For any detected instability flags will be set for quality control and diagnostics (to be modified after ground measurement data is available)

2.1) The standard deviation of the feedback SiPD > 0.10% of the averaged current value.

2.2) The standard deviation of the SRCA lamp current > 0.02% in constant current mode.

2.3) The standard deviation of the SRCA lamp voltage > 0.06% of the nominal voltage in constant current mode.

2.4) The standard deviation of the temperature of the feedback SiPD > 1K.

References

[1] “Broadband radiometry with spectrally selective detectors”, Optical Letter, 5(5):208-210, by J.M. Palmer and M.G. Tomasko, 1980.
[2] “SRCA VIS/NIR/SWIR radiance energy source approach”, SBRC Internal Memorandum, PL3095-N00536, by J. Young, Jan. 1992.
[3] “MODIS-N SRCA baseline design”, SBRC Internal Memorandum, PL3095-Q01118, by E. Johnson, May, 1992.
[4] “Radiometric stability of SRCA VIS/SWIR source”, SBRC Internal Memorandum, PL3095-Q02071, by E. Johnson, Jan. 1993.
[5] “MODIS MCST calibration presentation”, SBRC, Mar. 1993.
[6] “Halogen lamp de-rating requirement”, SBRC Internal Memorandum, PL3095-Q02806, by E. Johnson, July 1993.
[7] “Modeling and testing of SRCA SIS radiant output”, SBRC Internal Memorandum, PL3095-Q03202, by E. Johnson, Oct. 1993.
[8] “SRCA calibration algorithm”, SBRC Internal Memorandum, PL3095-Q03146, by E. Johnson, Oct. 1993.
[9]”Critical design review for the Moderate Resolution Imaging Spectroradiometer (MODIS)”, SBRC, Jan. 1994.
[10] “Follow-up stray light work on the SRCA assembly”, SBRC Internal Memorandum, PL3095-Q03692, by Terry Ferguson, Mar. 1994.
[11] “Inspection of 1-watt lamps for MODIS SIS”, SBRC Internal Memorandum, PL3095-Q04066, by Jon Mello , June 1994.
[12] “Polarized Source Assembly (PSA) simulation modeling”, SBRC Internal Memorandum, PL3095-N04230, by J. Young, Sep. 1994.
[13] “Spherical Integrator Source, SIS(100) radiometric model simulation”, SBRC Internal Memorandum, PL3095-N04231, by J. Young, Sep. 1994.
[14] “ATBD for MODIS level 1B algorithm”, MODIS algorithm team (MAT), Dec. 1994.
[15] “Predicted life of SRCA halogen lamps”, SBRC Internal Memorandum, PL3095-Q04694, by E. Johnson, Feb. 1995.
[16] “Science team action item - SRCA secondary mirror photodiode consideration”, SBRC Internal Memorandum, PL3095-Q04995, by E. Johnson, May 1995.
[17] “Software Requirements Specification for the MODIS Level 1B Software System”, P200-CD-001-001, MODIS Characterization Support Team, June 15, 1995.
[18] “Response to SRCA halogen lamp concerns”, SBRC Internal Memorandum, PL3095-Q05277, by E. Johnson, Aug. 1995.
[19]”MODIS calibration peer review data package”, SBRC, Aug. 1995.
[20] “Preliminary SRCA STOP analysis (reduced version)”, by Q.Gong, SAI, dtd., Aug. 1995.
[21] “MODIS operations concept document [M0007]”, by K. Parker and Ed. Knight, Nov. 1995.

[22] “MODIS level 1B Algorithm Theoretical Basis Document 1995 [MOD-02], M.Jones, H. Montgomery, R.Veiga, D. Knowles Jr., N. Che, L. Goldberg, Dec.1995.

[23] “ SRCA radiometric calibration algorithm”, SBRC Internal Memorandum, PL3095-Q05746, by R. Osgood, May 1996.

[24] “MODIS level 1B Algorithm Theoretical Document1996, M.Jones, H. Montgomery, R.Veiga, D. Knowles Jr., N. Che, L. Goldberg, Dec. 1996.

[25] “PC17 radiometric characterization, pre-thermal vacuum, ”, SBRC Internal Memorandum, PL3095-Q06330, by E. Johnson, Feb. 1997.

4. The SRCA in spectral mode

4.1 Physics of problem

Spectral characterization for MODIS is needed because of the spectral shifts observed in the solar reflective band filters during ground testing of MODIS precursor instruments, and because some on-orbit measurements from precursor instruments have been interpreted as showing evidence of on-orbit spectral shift.

During prelaunch TV testing, the center wavelengths of the MODIS bands are measured using Ground Support Equipment (GSE). An external double monochromator/collimator system fills the full MODIS aperture. The SRCA will be used to measure the center wavelength under similar conditions, and at very near the same time. Because the SRCA only partially fills the MODIS aperture, the center wavelengths measured by the SRCA may differ slightly from those measured by the GSE. Correction coefficients will be measured prelaunch to relate the measurement results from the GSE to those from the SRCA. These coefficients, which are band and channel dependent, are assumed to be unchanged on-orbit.

When the SRCA is operated in spectral mode, the grating motor turns the plain mirror used in radiometric/spatial mode 180° out of position and places the grating in position. Meanwhile, the slit/reticle motor places the entrance and exit slits in position. Thus, the calibration SiPD, located at the secondary slit behind a piece of didymium glass starts collecting signals. The secondary slit is in parallel with the main exit slit, separated by six millimeters with a calibration SiPD behind it. When the grating is rotating, the spectrum disperses along the slit width. A narrow spectral beam exits the slits.

The spectral beam exited from the main exit slit is sampled by a reference SiPD located at the center of the secondary mirror of the Cassegrain telescope to provide normalizing signals. The main portion of the beam is further collimated by the Cassegrain telescope to form a collimated beam and folded towards the MODIS scan mirror by a plain mirror. The spectral beam exited from the secondary slit passes through the didymium glass and is detected by the calibration SiPD. The reference and the calibration SiPDs are selected in pairs with the same spectral responsivity. The two sets of signals form the data base for wavelength calibration.

The wavelength self-calibration capability depends upon the optical properties of the didymium glass. The wavelength location of the transmission peaks of the didymium glass is assumed to be unchanged with temperature. The signals from the calibration SiPD behind the didymium glass are what we call the spectrum modified by the didymium transmission curve while the signals from the reference SiPD are the spectrum itself. The calibration SiPD signal shape, after dividing by the reference SiPD signals, will

be the same as the didymium transmission curve. However, the location difference of the two SiPDs complicates the signal processing.

The radiance of the monochromatic beam illuminating the MODIS detectors is spectral-dependent. The beam is spectrally modified by the SRCA SIS light source, the grating efficiency, the SRCA transmittance, and the reflectivity of the mirror. In-order to recover the MODIS band response for accurately determining the center wavelength and the bandwidth, the MODIS detector signals need to be normalized by the spectral-dependent signals from the SRCA. The reference SiPD provides the normalization signal except that the reference SiPD signals include the modification of the SiPD spectral response. Further processing of the normalized signals is imperative. Due to the limitation of the reference SiPD response, the normalization can only performed for wavelengths less than 1μm. For the bands with spectral response greater than 1μm the MODIS detector signals are not normalized. For bands with center wavelength greater than 1 μm the accuracies of the center wavelength and bandwidth are not addressed in the MODIS specification to SBRS.

Compared to broad-band, the use of a monochromatic beam in spectral calibration results in low illumination level to MODIS. The lamp configurations used in spectral calibration will differ from those used in radiometric calibration. Two lamp configurations are utilized: 3-10W and 1-10W. The 1-1W lamp is not used because the signal would be too low. Two 10W lamp configuration has been canceled for saving both the grating motor and lamp life. The lamp configuration for each MODIS band depends on the best SNR and the possible range of grating angles.

There is no demonstrated method for validating the spectral characteristics of MODIS on-orbit using ground verification methods.

4.2 Allocation of grating angles for MODIS bands in unidirectional rotation for each lamp configuration

The grating directs a beam with narrow spectral bandwidth centered at a specific wavelength through the exit slit. The grating stepping motor rotates the grating unidirectionally for each lamp configuration. During one cycle of grating rotation (less than 9.5 degrees), the exit spectrum should cover both the spectral response of certain MODIS bands and the wavelength ranges of the didymium peaks to be measured. We need to measure at least two didymium peaks in one grating unidirectional rotation. Three didymium peaks is actually in use. In summary, all twenty bands (1-19 and 26) and six didymium peaks should be measured in the two unidirectional rotations.

The nominal values of the monochromator parameters are [18]:

- The half angle between the incident beam to the grating and the diffracted beam exited from the main exit slit in the diffraction plane. It is called half included angle for simplicity, $\beta = 15°$.

- Grating motor offset angle, $\theta_{off} = 0°$

The values of some other parameters are [18]:

- grating spacing, $A = 4.240882$ μm (235.8 grooves per millimeter).
- Angular displacement between the main exit slit and the didymium slit, $\Delta = 1.319°$
- Stepping motor increment: 0.00588235° in average.

Different wavelengths, λ, λ/2, λ/3, etc. will be spatially overlapped for a specific grating angle. Order sorting filters are inserted between the SRCA SIS and the relay mirror. It filters out the unwanted wavelengths and retains only the wavelength needed. There are three order-sorting filters mounted in the SRCA filter wheel. The spectral ranges for the three filters are as follows: No.1 filter for transmission range of 0.40 - 0.52 μm, No.2 for 0.52 - 0.70 μm, and No.3 for 0.73 - 0.99 μm. The open hole is called No.0 (zero). The choice of filters depends on the grating angle and the diffraction order in use.

The wavelength of the monochromatic beam exiting from the main slit is related to the grating angle by the grating equation

$$\lambda = \frac{2A}{m}\sin(\theta_M + \theta_{off})\cos\beta \qquad (4.2.2)$$

The wavelength of the monochromatic beam exited from the didymium slit is

$$\lambda = \frac{2A}{m}\sin(\theta_M + \theta_{off} + \frac{\Delta}{2})\cos(\beta + \frac{\Delta}{2}) \qquad (4.2.3)$$

We also need to know the locations of the transmission peaks of the didymium glass. The transmittance of didymium glass is shown in Figure 4.2.1, where six sharp transmission peaks are marked by D1 - D6. The algorithm uses various combinations of didymium peaks and diffraction orders. In Table 4.2.1 we define the following combination ***Dlm***, where ***l*** designates diffraction order and ***m*** designates transmission peak number.

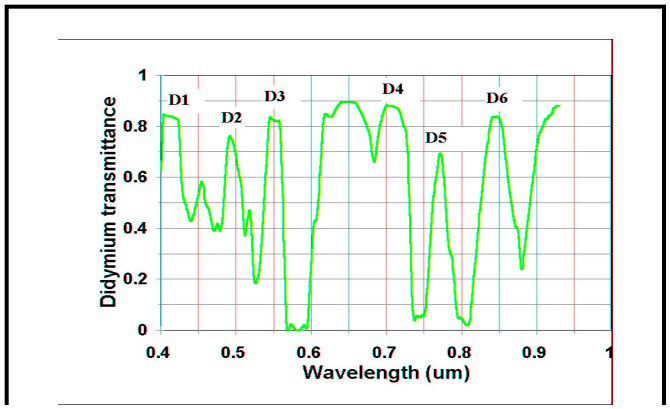

Figure 4.2.1 Transmittance of didymium glass

Table 4.2.1 Didymium peak location

Didymium peak	Wavelength (μm)	Bandwidth (nm)	Diffraction order
D31	0.415	25	-3
D32	0.496	25	-3
D23	0.551	30	-2
D33	0.551	30	-3
D24	0.707	40	-2
D25	0.772	25	-2
D26	0.846	35	2

Based upon the nominal data and Eqs. (4.2.2) and (4.2.3), the values of grating angles corresponding to the didymium peaks and the MODIS bands in unidirectional rotation for each lamp configuration are listed in Table 4.2.2. Since the calibration and the reference SiPDs are located at different positions, the grating angle values to cover the same wavelength are at different grating angles. Thus, the grating angle range must include both the main exit slit range and the didymium peaks which are in two different rows of the table with '*" for didymium slit and without "*" for main slit. The calibration signals can be normalized by the reference signals in the same wavelength range and didymium peak position can be calculated. For simplicity, only one order sorting filter is permitted for each grating angle. Grating angle overlapping for different diffraction orders is not permitted in that case the order-sorting filters would have to flip back and forth at the same grating angle. In table 4.2.2 the step size of the grating motor depends on the band width or didymium peak width in order to have more than 25 data samples (No. of step). The number of samples per step depends on the SNR. The lower the SNR, the higher the number of samples per step.

Figure 4.2.2 shows the MODIS band responses and the diffraction orders in terms of grating motor angle. The horizontal bar corresponding to each band shows the associated diffraction order.

Table 4.2.2 Allocation of grating angle for each unidirectional rotation

Band	Wvln	Band width	Filtr No.	Diff. order	Wavelength range		Grating angle		Step number		Step size	No. of step	sample per step, N_{scan}
					Min.	Max.	Min.	Max.	Min.	Max.			
1-10W lamp configuration													
19	0.935	0.048	3	-1	0.906	0.965	6.346	6.766	31679	31751	3	25	2
D23 D23*	0.551	0.030	2	-2	0.531	0.570	7.450 6.820	8.004 7.364	31868 31760	31961 31853	3 3	32 32	8 8
12	0.547	0.011	2	-2	0.540	0.554	7.575	7.774	31889	31922	1	34	2
5	1.240	0.020	0	-1	1.227	1.254	8.615	8.804	32065	32098	1	34	2
13	0.665	0.010	2	-2	0.659	0.672	9.252	9.445	32173	32206	1	34	2
14	0.677	0.011	2	-2	0.669	0.684	9.405	9.619	32199	32236	1	38	2
26	1.375	0.030	0	-1	1.356	1.396	9.525	9.809	32220	32268	2	25	2
D32 D32*	0.496	0.025	1	-3	0.481	0.512	10.14 9.514	10.80 10.17	32324 32218	32436 32330	4 4	29 29	8 8
15	0.746	0.010	3	-2	0.739	0.754	10.40	10.60	32369	32402	1	34	2
D33 D33*	0.551	0.030	2	-3	0.532	0.570	11.23 10.61	12.04 11.41	32510 32404	32646 32540	4 4	35 35	8 8
6	1.640	0.024	0	-1	1.627	1.655	11.45	11.65	32547	32582	1	36	2
16	0.866	0.016	3	-2	0.855	0.877	12.04	12.36	32647	32701	2	28	2
18	0.935	0.014	3	-2	0.926	0.945	13.06	13.34	32821	32869	2	25	2
7	2.130	0.050	0	-1	2.100	2.161	14.85	15.29	33125	33200	3	26	2
3-10W lamp configuration													
D23 D23*	0.551	0.030	2	-2	0.531	0.570	7.450 6.820	8.004 7.364	31868 31760	31961 31853	3 3	32 32	2 2
4	0.553	0.020	2	-2	0.541	0.566	7.581	7.941	31890	31950	2	31	2
8	0.412	0.014	1	-3	0.402	0.421	8.469	8.863	32040	32108	2	35	40
1	.0644	0.050	2	-2	0.616	0.673	8.656	9.456	32072	32208	4	35	4
9	.0442	0.011	1	-3	0.435	0.450	9.163	9.480	32158	32212	2	28	4
3	.0466	0.019	1	-3	0.452	0.479	9.537	10.10	32222	32318	4	25	24
10	0.487	0.011	1	-3	0.480	0.494	10.11	10.43	32320	32374	2	28	2
D32 D32*	0.496	0.025	1	-3	0.481	0.512	10.14 9.514	10.80 10.17	32324 32218	32436 32330	4 4	29 29	2 2
D33 D33*	0.551	0.030	2	-3	0.532	0.570	11.23 10.61	12.04 11.41	32510 32404	32646 32540	4 4	35 29	2 2
11	0.530	0.012	2	-3	0.522	0.538	11.02	11.36	32474	32532	2	30	2
2	0.855	0.037	3	-2	0.834	0.879	11.75	12.39	32598	32706	4	28	2
17	0.904	0.034	3	-2	0.885	0.924	12.47	13.04	32721	32817	3	33	2

Note: The grating angles and motor step numbers corresponding to Dlm*(D23*, D32*, D33*) are used for acquiring the same wavelength range from the didymium slit.

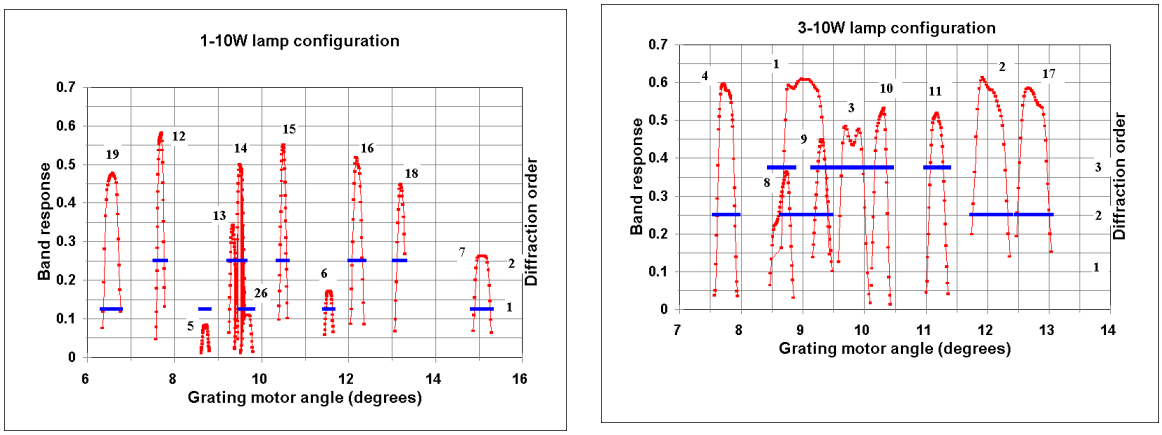

Figure 4.2.2 MODIS band response in terms of grating motor angle

4.3 Mathematical description of the algorithm

Spectral calibration starts by collecting the signals of the reference SiPD, calibration SiPD, and the MODIS detectors. For each step of grating rotation, the scan mirror rotates a number of scans, N_{scan}. The N_{scan} is varied from band to band for the best SNR in the spectral measurement. Since the main exit slit image fills approximately half of the 1 km IFOV detector size, only 2 or 3 data frames are available for processing.

The SRCA spectral self-calibration requires that two monochromator parameters, β_L and $\theta_{off,L}$, be determined from measured data for each unidirectional rotation of the grating.

The flow chart of the SRCA spectral calibration is shown in Figure 4.3.1.

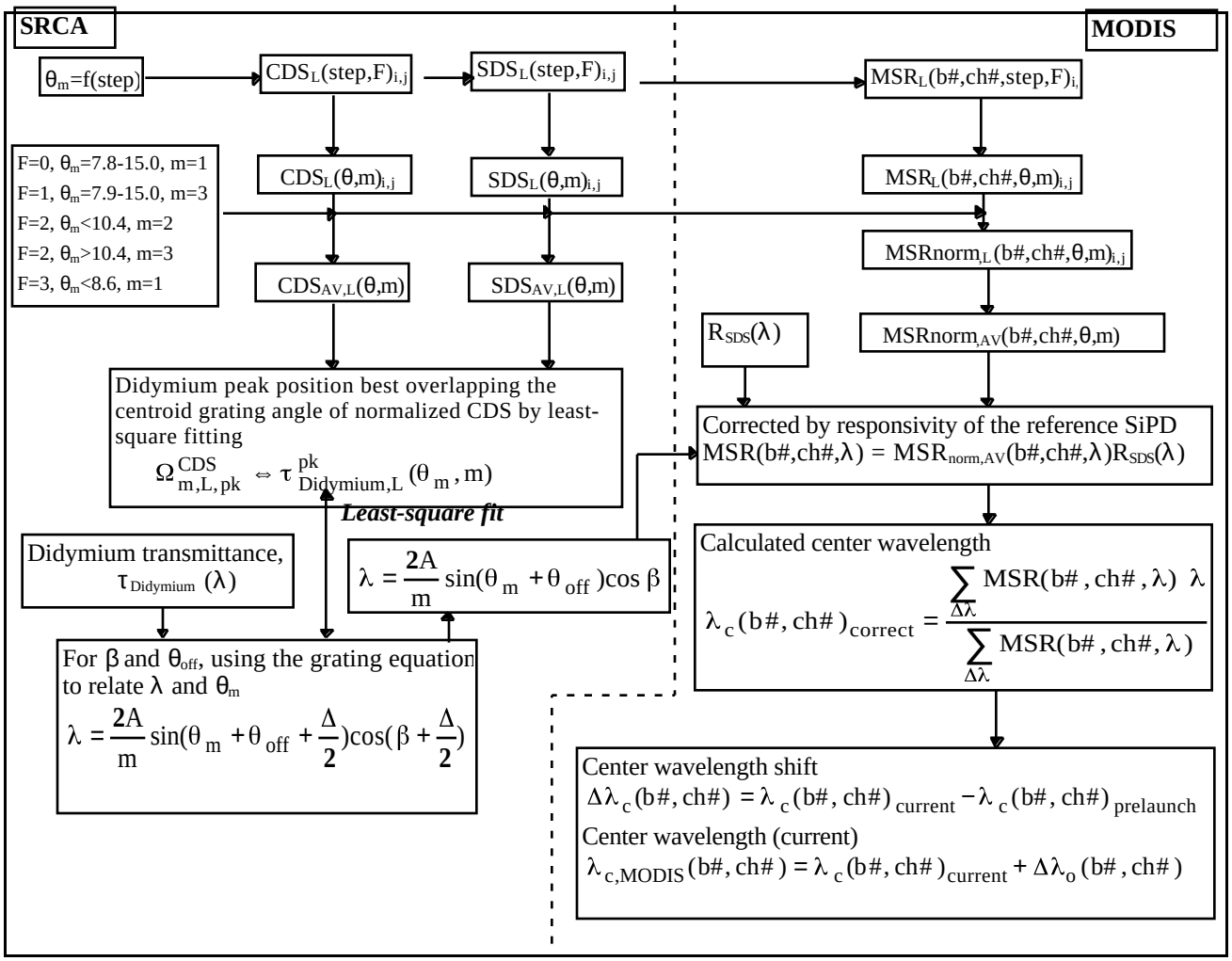

Figure 4.3.1 Flow chart for spectral calibration using the SRCA

4.3.1 Convert grating motor step number to grating angle using the ground measurement data base

Signals collected for each grating step are: calibration signal from the calibration SiPD, $CDS_L(step,F)_{scan,\ Frame}$, reference signal from the reference SiPD, $SDS_L(step,F)_{scan,\ Frame}$, and signal of the MODIS detectors, $MSR_L(b\#,ch\#,step,F)_{scan,Frame}$. The subscript ***L*** is the lamp configuration, ***step*** is the grating motor step number, ***F*** is the order-sorting filter number, ***b#*** is the band number, ***ch#*** is the channel number, the subscript "***scan***" is the scan number, and the subscript "***frame***" is the frame number. In Figure 4.3.1 the subscripts of i,j are used in corresponding to "***scan***" and "***frame***".

For simplicity in writing the algorithm, we assume that the MODIS detector signals have been corrected for detector non-linearity, temperature-related change, scan angle effect, scan mirror reflectivity, and the space count has been subtracted. We also assume that the SRCA reference and calibration SiPD signals have been corrected for non-linearity and the dark signals have been subtracted. A set of 26 dark DN values are taken before and after the lamps are on. The dark currents of the reference / calibration SiPDs are the average of the 52 (2 × 26) data points.

Using the prelaunch data base (Figure 4.3.2), the grating motor step number is transferred to grating angle, θ_M by

$$\theta_M = f(step) \tag{4.3.1}$$

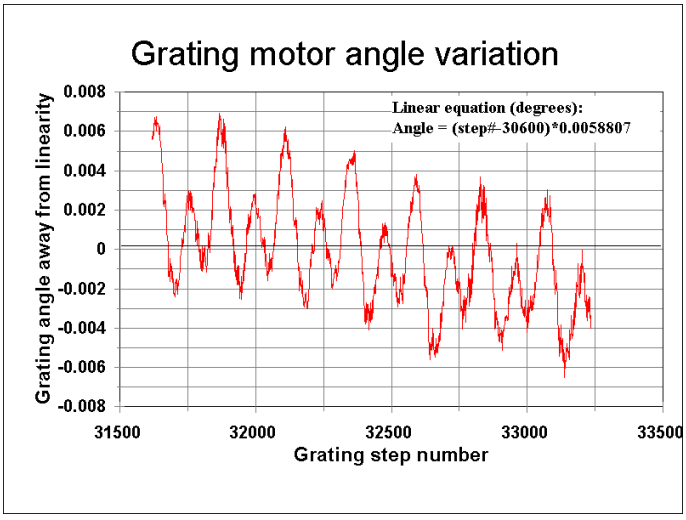

Figure 4.3.2 Grating angle as a function of motor step number

The non-linearity for the grating motor angle [16] is illustrated in Figure 4.3.2.

4.3.2 Determine the diffraction order, m, to be used according to the order-sorting filter number, F, and the step motor angle, θ_M

The filter number, F, is fixed prelaunch corresponding to the grating angle for each lamp configuration. The diffraction order is determined according to the relationship listed in Table 4.3.1.

Table 4.3.1 Convert filter number to diffraction order

Order-sorting filter number, F	Step motor angle, θ_M (degrees)	Diffraction order, m
0 (open)	7.8 - 15.0	1
1	7.8 - 15.0	3
2	< 10.4	2
2	> 10.4	3
3	< 8.6	1
3	> 8.6	2

4.3.3 Average the signals of the calibration SiPD and the reference SiPD over number of scans and frames.

$$CDS_{AV,L}(\theta_m, m) = \frac{1}{N_{Scan} \cdot N_{Frame}} \sum_{1}^{N_{Scan}} \sum_{1}^{N_{Frame}} CDS_L(\theta_m, m)_{Scan,Frame} \qquad (4.3.2)$$

$$SDS_{AV,L}(\theta_m, m) = \frac{1}{N_{Scan} \cdot N_{Frame}} \sum_{1}^{N_{Scan}} \sum_{1}^{N_{Frame}} SDS_L(\theta_m, m)_{Scan,Frame} \qquad (4.3.3)$$

for N_{scan} refer to Table 4.2.2.

4.3.4 Physically shift the reference signals

For a given encoder angle the two signals, the calibration SiPD and the reference SiPD, are at different wavelengths because they are measured at different locations. Their wavelength expressions have been given in Eqs. (4.2.2) and (4.2.3).

In order to ratio the two signals with the same wavelength scale, we express the step motor angle for the reference SiPD as θ'_{M}. Set the wavelength in Eqs. (4.2.2) and (4.2.3) equal and we have

$$\theta'_{M,pk} = \sin^{-1}\left[\frac{\cos(\beta_o + \Delta/2)}{\cos\beta_o}\sin(\theta_{M,pk} + \Delta/2 + \theta_{offo})\right] - \theta_{offo} \qquad (4.3.4)$$

where the subscript "***o***" designates prelaunch data. The use of prelaunch values introduces negligible error because the two variables, β and θ_{off}, change slightly and the error in $\theta'_{M,pk}$ is less than one angular motor step. Because we consider only the step motor angle at the didymium peaks, a subscript "***pk***" is added with step motor angle hereafter.

The angle $\theta'_{M,pk}$ is very close to $\theta_{M,pk}+\Delta/2$. Eq.(4.3.4) is used to compute $\theta'_{M,pk}$ and then converted to an integer number of motor step.

Calculation of $\theta'_{M,pk}$ is limited to the didymium peak regions utilized. The starting and ending angles of $\theta_{M,pk}$ and $\theta'_{M,pk}$ for signal normalization are provided in the data base.

4.3.5 Normalization of the calibration SiPD signals by the reference SiPD signals

The normalized calibration SiPD signals are

$$CDS_{norm,L}(\theta_{M,pk}, m) = \frac{CDS_{AV,L}(\theta_{M,pk}, m)}{SDS_{AV,L}(\theta'_{M,pk}, m)} \qquad (4.3.5)$$

The normalization of CDS also removes the temperature effect assuming that the two SiPDs have the same temperature coefficients because they are all mounted in the SRCA housing.

The centroid wavelength of the didymium transmission peak is calculated over the peak region, starting from $\lambda_{1,pk,L}$ to $\lambda_{2,pk,L}$, by

$$\lambda_{didymium,pk,L} = \frac{\sum_{\lambda_{1,pk,L}}^{\lambda_{2,pk,L}} \tau_{didymium}(\lambda)\cdot\lambda}{\sum_{\lambda_{1,pk,L}}^{\lambda_{2,pk,L}} \tau_{didymium}(\lambda)} \qquad (4.3.6)$$

The centroid step motor angle of the transmission peak is the normalized calibration signals weighted by the step motor angle range and summed from $\theta_{M1,pk}$ to $\theta_{M2,pk}$ given in the prelaunch data base.

$$\Omega^{CDS}_{m,pk,L} = \frac{\sum_{\theta_{M1,pk,L}}^{\theta_{M2,pk,L}} CDS_{norm,L}(\theta_{M,pk}, m)\cdot\theta_{M,pk,L}}{\sum_{\theta_{M1,pk,L}}^{\theta_{M2,pk,L}} CDS_{norm,L}(\theta_{M,pk}, m)} \qquad (4.3.7)$$

The computed wavelength corresponding to the centroid step motor angle, $\Omega^{CDS}_{m,pk,L}$, is

$$\lambda^{CDS}_{pk,L} = \frac{2A}{m}\sin(\Omega^{CDS}_{m,pk,L} + \theta_{off,L} + \Delta/2)\cos(\beta_L + \Delta/2) \qquad (4.3.8)$$

where ***m*** uses positive value (the same as follows) because Eq.(4.3.8) should have a negative sign on the left side and ***m*** in actual use is negative.

If the monochromator parameters, β_L and $\theta_{off,L}$, are determined correctly, the $\lambda^{CDS}_{pk,L}$ will equal the computed value $\lambda_{didymium,pk,L}$.

A least-square fit technique [17] is utilized to adjust β_L and $\theta_{off,L}$ until the $\lambda^{CDS}_{pk,L}$ best fits $\lambda_{didymium,pk,L}$ at a number of peaks, N_{peak}, in use. The following outlines the procedure.

Starting with the grating equation (see Eq.(4.3.8)), we assume that

$$C_1 = 2A\cos(\beta_L + \Delta/2); \qquad C_2 = \theta_{off,L} + \Delta/2. \qquad (4.3.9)$$

Eq.(4.3.9) becomes

$$m\lambda_{didymium,pk,L} = m\lambda^{CDS}_{pk,L} = C_1\cdot\cos C_2\cdot\sin\Omega^{CDS}_{m,pk,L} + C_1\cdot\sin C_2\cdot\cos\Omega^{CDS}_{m,pk,L} \qquad (4.3.10)$$

In order to have a linear fit, set

$$a(1)\cdot func(1) = C_1\cdot\cos C_2\cdot\sin\Omega^{CDS}_{m,pk,L} \qquad (4.3.11)$$

and

$$a(2)\cdot func(2) = C_1\cdot\sin C_2\cdot\cos\Omega^{CDS}_{m,pk,L} \qquad (4.3.12)$$

where

$$a(1) = C_1\cos C_2; \quad a(2) = C_1\sin C_2 \qquad (4.3.13)$$

$$func(1) = \sin\Omega^{CDS}_{m,pk,L}, \text{ and } func(2) = \cos\Omega^{CDS}_{m,pk,L} \qquad (4.3.14)$$

The result of linear fit by $\Omega_{m,pk,L}^{CDS}$ and $m\lambda_{didymiu,pk,L}$, gives ***a(1)*** and ***a(2)*** (see **svdfit.f** in "Numerical Recipe"). From the Eqs.(4.3.11) and (4.3.12), the two monochromator parameters can be determined.

$$\theta_{off,L} = tan^{-1}\left(\frac{a(2)}{a(1)}\right) - \frac{\Delta}{2} \tag{4.3.15}$$

$$\beta_L = cos^{-1}\left(\frac{a(1)}{2Acos(\theta_{off,L} + \frac{\Delta}{2})}\right) - \frac{\Delta}{2} \tag{4.3.16}$$

4.3.6 Normalize the MODIS detector signals by the reference SiPD signals

The purpose of the normalization is to eliminate the effects of the spectral shape of the light source on the center wavelength and bandwidth measurements.

$$MSR_{Norm,L}(b\#, ch\#, \theta_M, m)_{scan,\,frame} = \frac{MSR_L(b\#, ch\#, \theta_M, m)_{scan,\,frame}}{SDS_L(\theta_M, m)_{scan,\,frame}} \tag{4.3.17}$$

This normalization is not proper because the $SDS_L(\theta_M, m)_{scan,frame}$ includes not only the spectral shape of the light source but also the spectral response of the reference SiPD. Correction for the spectral shape of the reference SiPD is introduced in section 4.3.8.

4.3.7 Average the MODIS detector signals over the number of scans and frames

$$MSR_{Norm,AV,L}(b\#, ch\#, \theta_M, m) = \frac{1}{N_{Scan} \cdot N_{Frame}} \sum_{1}^{N_{Scan}} \sum_{1}^{N_{Frame}} MSR_{norm,L}(b\#, ch\#, \theta_M, m)_{Scan,Frame} \tag{4.3.18}$$

4.3.8 Convert the MODIS detector signals in terms of step motor angle into a function of wavelength and further correct for the spectral responsivity of the reference SiPD

The current monochromator parameters, β_L and $\theta_{off,L}$, resulting from converged values in Eq. (4.3.15 and 4.3.16), are utilized in the grating equation to convert step motor angle to wavelength of light from the SRCA

$$\lambda = \frac{2A}{m} sin(\theta_M + \theta_{off,L}) cos\beta_L \tag{4.3.19}$$

The average normalized MODIS signal, $MSR_{Norm,AV,L}(b\#,ch\#,\theta_M,m)$, is converted to $MSR_{Norm,AV,L}(b\#,ch\#,\lambda)$. After correction by the spectral responsivity of the reference SiPD, $R_{SDS}(\lambda)$, and the temperature-related effect, the normalized MODIS detector signals are

$$MSR_L(b\#,ch\#,\lambda) = MSR_{Norm,AV,L}(b\#,ch\#,\lambda)\cdot R_{SDS}(\lambda)\cdot(1+\Delta R_{SDS}(\lambda,T)\cdot(T-T_o)) \tag{4.3.20}$$

where $\Delta R_{SDS}(\lambda,T)$ is the temperature coefficient of the reference SiPD. T is the current reference SiPD temperature which uses the temperature value measured at the secondary mirror of the SRCA and T_o is the temperature at which the $R_{SDS}(\lambda)$ is measured.

Notice that the relationship in Eq.(4.3.19) is related to the lamp configuration. When using Eq.(4.3.20) for a particular band, the same lamp configuration must be used throughout the process.

4.3.9 Determine the center wavelength for each MODIS band

The center wavelength, λ_c, of each MODIS detector is

$$\lambda_c(b\#,ch\#)_{current} = \frac{\sum_{\lambda_{1(b\#)}}^{\lambda_{2(b\#)}} MSR_L(b\#,ch\#,\lambda)\cdot\lambda}{\sum_{\lambda_{1(b\#)}}^{\lambda_{2(b\#)}} MSR_L(b\#,ch\#,\lambda)} \tag{4.3.21}$$

4.3.10 Determine the center wavelength shift and current center wavelength

The center wavelength shift is the difference between the current center wavelength measured by the SRCA on-orbit and that measured prelaunch by the SRCA in TV.

$$\Delta\lambda_c(b\#,ch\#) = \lambda_c(b\#,ch\#)_{current} - \lambda_c(b\#,ch\#)_{prelaunch} \tag{4.3.22}$$

The center wavelength measured by the GSE during TV testing is slightly different from that measured by the SRCA due to the SRCA partial aperture filling. The difference is assumed unchanged on-orbit. The center wavelength correction item is

$$\Delta\lambda_o(b\#,ch\#) = \lambda_c(b\#,ch\#)_{GSE} - \lambda_c(b\#,ch\#)_{SRCA} \tag{4.3.23}$$

The center wavelength shift for a designated band is

$$\Delta\lambda_c(b\#) = \frac{1}{N_{ch}(b\#)} \sum_{1}^{N_{ch}(b\#)} \Delta\lambda_c(b\#, ch\#) \tag{4.3.24}$$

The current center wavelength is

$$\lambda_c(b\#, ch\#) = \lambda_c(b\#, ch\#)_{current} + \Delta\lambda_o(b\#, ch\#) \tag{4.3.25}$$

The current center wavelength for a designated band is

$$\lambda_c(b\#) = \frac{1}{N_{ch}(b\#)} \sum_{1}^{N_{ch}(b\#)} \lambda_c(b\#, ch\#) \tag{4.3.26}$$

where $N_{ch}(b\#)$ is the number of channels of band ***b#.***

4.3.11 Determine the band width

The band width is defined here as the width between cut-in and cut-off wavelengths. The $\lambda_{cut\text{-}in}$ and $\lambda_{cut\text{-}off}$ are corresponding to the wavelengths where MODIS signal is at the half maximum responses, $0.5MSR_L(b\#,ch\#,\lambda)_{max}$, for a band/channel. The band width is

$$\Delta\lambda(b\#, ch\#) = \lambda_{cut-off}(b\#, ch\#) - \lambda_{cut-in}(b\#, ch\#) \tag{4.3.27}$$

The band width for a designated band is

$$\Delta\lambda(b\#) = \frac{1}{N_{ch}(b\#)} \sum_{1}^{N_{ch}(b\#)} \Delta\lambda(b\#, ch\#) \tag{4.3.28}$$

4.4 Uncertainty estimates

The uncertainty estimate is given in Table 4.4.1. The wavelength measurement accuracy prelaunch is determined by the spectral resolution of the GSE(0.33 nm). The center wavelength will be measured using the SRCA in TV. An additional uncertainty of 0.32 nm will be the result.

Table 4.4.1 Uncertainty estimate of spectral calibration using the SRCA

Item	Description of error sources	Uncertainty	Band 8 case
1	GSE(1)		0.33 nm
2	Transfer from GSE to MODIS (1)		0.32 nm
3	Grating motor angle repeatability and non-linearity [5]	6 arc sec.	0.08 nm
4	Grating width error in manufacturing [5]	0.10 nm	0.05 nm
5	Half included angle between entrance and exit slits, $d\beta$, of $\pm 0.24°$ and grating motor offset, $d\theta_{off}$, of $\pm 0.014°$ (2)		0.28 nm
Total	(at confidence level 1 σ)		0.54 nm

Item	Description of error sources	Uncertainty
7.1	Grating width error due to temperature change of 20K (1)	0.12 nm
7.2	SRCA focal length	0.5 mm
7.3	Difference in spectral responsivity of reference and calibration SiPDs	0.25%
7.4	Lamp output variation and drift	0.25%
7.5	Limited sampling step	determined by algorithm
7.6	Correction coefficient due to SRCA partial aperture illumination	no change
7.7	Potential diverge in spectral response of the reference/calibration SiPDs on-orbit	no change
7.8	Quantization and SNR	1/DN/√No. averaged

(1) From SBRC

(2) These errors result from the uncertainties given in 7.1 -- 7.8. Error in β and θ_{off} subsequently cause error in wavelength through the grating equation.

The uncertainty of the center wavelengths for MODIS bands (1-19 and 26) is given in Figure 4.4.1. The uncertainty increases significantly for band 5, 6, 7, and 26 because the MODIS detector signal can not be normalized due to the lack of SiPD response in their wavelength range. Wavelength uncertainty decreases with increasing diffraction order utilized. However, these uncertainties will be reduced when using the center wavelength

shift information in comparison with prelaunch results because the bias for the center wavelength measurement due to the use of un-normalized the MODIS detector signals will be basically canceled out. Although the two SiPDs are manufactured at the same lot and the spectral response are well matched, we have no experience how the characteristics may change on-orbit. Divergence of the reference SiPD characteristics from the calibration SiPD's will undoubtedly contribute uncertainty to the calibration.

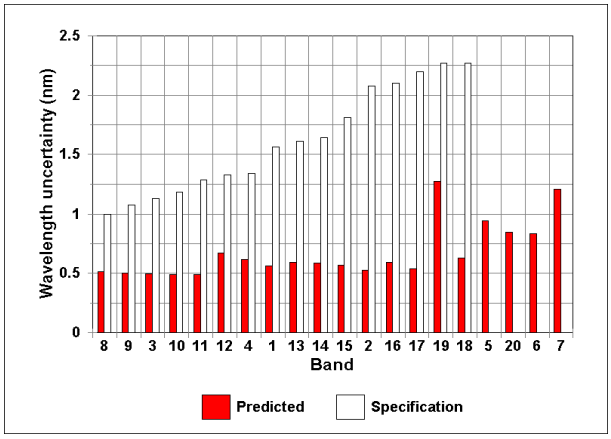

Figure 4.4.1 Uncertainty in spectral calibration using the SRCA

4.5 Description of input data set, output products, and quality control

4.5.1 Input data set

The database for input to the algorithm includes:

(1) The spectral transmittance of the didymium absorption glass, $\tau_{didymium}(\lambda)$

(2) The spectral transmittance of the three order-sorting filters, $\tau_{order}(\lambda)$

(3) The lookup table of grating angles vs. the grating motor steps, $\theta_M = f(step)$

(4) The spectral response of the calibration and the reference SiPDs, $R_{CDS}(\lambda)$ and $R_{SDS}(\lambda)$

(5) The temperature coefficients for the reference SiPD in terms of wavelength and temperature, $\Delta \boldsymbol{R_{SDS}(\lambda,T)}$

(6) The correction coefficients for the SRCA partial aperture filling effect in TV, $\Delta\lambda_{\boldsymbol{o}}\boldsymbol{(b\#,ch\#)}$

(7) The center wavelength values for each MODIS solar reflective band in TV, $\lambda_{\boldsymbol{c}}\boldsymbol{(b\#,ch\#)_{prelaunch}}$

(8) Monochromator parameters measured prelaunch (Grating width, ***A***, half included angle, $\beta_{\boldsymbol{o}}$, grating motor offset, $\theta_{\boldsymbol{offo}}$, angular displacement between main exit slit and didymium slit, Δ, the SRCA focal length, ***f***, and other structure parameters)

(9) Non-linearity coefficients for the SRCA calibration and reference SiPDs

(10) Signal thresholds for setting instability flags (DNs for MODIS detectors, space count, the calibration and reference SiPDs)

(11) The spectral response of MODIS detectors, $\boldsymbol{R_{b,ch}(\lambda)}$

4.5.2 Output products

(1) Center wavelength shift, $\Delta\lambda_{\boldsymbol{c}}\boldsymbol{(b\#,ch\#),}$ for each MODIS band/channel (band 1-19 and 26)

(2) Band center wavelength shift, $\Delta\lambda_{\boldsymbol{c}}\boldsymbol{(b\#)}$ and standard deviation.

(3) Center wavelength, $\lambda_{\boldsymbol{c}}\boldsymbol{(b\#,ch\#),}$ for each MODIS band/channel.
(4) Band center wavelength, $\lambda_{\boldsymbol{c}}\boldsymbol{(b\#)}$ and standard deviation.

(5) Off-line products for science team evaluation are

- The cut-in and cut-out wavelengths, $\lambda_{\boldsymbol{cut\text{-}in}}\boldsymbol{(b\#,ch\#)}$ and $\lambda_{\boldsymbol{cut\text{-}out}}\boldsymbol{(b\#,ch\#),}$ at half maximum response for each MODIS band/channel

- Band cut-in and cut-out wavelengths, $\lambda_{\boldsymbol{cut\text{-}in}}\boldsymbol{(b\#)}$ and $\lambda_{\boldsymbol{cut\text{-}out}}\boldsymbol{(b\#)}$ and standard deviation.

- Trending of MODIS spectral calibration results, $\Delta\lambda_c$***(b#,ch#)*** and λ_c***(b#,ch#),*** using the SRCA

4.5.3 Data report format

The following data should be tagged to the output products:

(1) Date and time

(2) Lamp configuration

4.5.4 Quality control

(1) At the grating steps where the DN is low, the DN will be averaged over multi-scans to improve the SNR (> 100).

(2) The flags will be set if: (to be modified after ground measurement data is available)

2.1) The same as items (2.1) - (2.4) in 3.4.4.

2.2) The feedback, reference, and calibration SiPDs are claimed as dead if $DN_{max} < 1.3\ DN_{dark} + 3\ \sigma$.

2.3) The temperature of the reference/calibration SiPD is out of range of characterization (< 15°C or > 35°C).

2.4) The reference/calibration SiPDs are saturated if DN > 4095.

2.5) The monochromator parameters, $d\beta > 0.5°$ and $\theta_{off} > 1$ step.

References

[1] “MODIS-N SRCA baseline design”, SBRC Internal Memorandum, PL3095-Q01118, by E. Johnson, May, 1992.

[2] “Optical design of the MODIS-N SRCA”, SBRC Internal Memorandum, PL3095-Q01117, by C. Welis, May 1992.

[3] “SRCA motor requirements (and operational scenarios”, SBRC Internal Memorandum, PL3095-Q01474, by E. Johnson, Aug. 1992.

[4] “Simulation of MODIS SRCA spectral calibration”, SBRC Internal Memorandum, PL3095-N01778, by J. Lanstng, Nov. 1992.

[5] “SRCA spectral measurement accuracy”, SBRC Internal Memorandum, PL3095-Q02020, by E. Johnson, Jan. 1993.

[6] “MODIS MCST calibration presentation”, SBRC, Mar. 1993.

[7] “SRCA tolerance analysis”, SBRC Internal Memorandum, PL3095-Q02340, by E. Johnson and R. Kebo, Mar. 1993.

[8] ”Critical design review for the Moderate Resolution Imaging spectroradiometer (MODIS)”, SBRC, Jan. 1994.

[9] “Preliminary MODIS spectral response curves”, GSFC, NASA, Jun. 1994.

[10] “Polarized Source Assembly (PSA) simulation modeling”, SBRC Internal Memorandum, PL3095-N04230, by J. Young, Sep. 1994.
[11] “SRCA spectral calibration methodology”, SBRC Internal Memorandum, PL3095-N04744, by J. young, Mar. 1995.
[12] “ATBD for MODIS level 1B algorithm”, MODIS algorithm team (MAT), Dec. 1994.
[13] “Software Requirements Specification for the MODIS Level 1B Software System”, P200-CD-001-001, MODIS Characterization Support Team, June 15, 1995.
[14] “MODIS operations concept document [M0007]”, by K. Parker and Ed. Knight, Nov. 1995.
[15] “MODIS level 1B Algorithm Theoretical Document 1995 [MOD-02]”, M. Jones, H. Montgomery, R. Veiga, D. Knowles Jr., N. Che, and L. Goldberg, Dec. 1995.
[16] “SRCA grating motor data”, SBRS Internal Memorandum, PL3095-Q05520, by E. Johnson, Nov. 1995.
[17] “SRCA spectral calibration algorithm”, SBRS Internal Memorandum, PL3095-Q05661, by R. Osgood, March. 1996.
[18] “Response to GSFC questions regarding MODIS OBCs”, SBRS Internal Memorandum, PL3095-Q05738, by E. Johnson, Apr. 1996.
[17] “Response to SRCA questions from GSFC”, SBRS Internal Memorandum, PL3095-Q06002, by E. Johnson, Aug. 1996.

5. The SRCA in spatial mode

5.1 Physics of problem

The 490 detectors for the 36 MODIS bands are located on four different focal planes. Their positions need to be measured on-orbit in order to determine their relative registration to each other and their ground footprint locations. Possible detector position shifts require measurement of the spatial position on-orbit.

Figure 5.1.1 is the layout of the four focal plane assemblies (FPA). The band number is marked under the detector arrays for each band. The scan and track directions are marked at the corner for each FPA as S and T, where S stands for along-scan and T for along-track. The relative positions along track of the bands in the four FPAs are shown in Figure 5.1.2. The actual location of the detectors along-scan relative to the left edge of band 32 is called Frame of Data (FD) in 1-km IFOV units. The band number is marked directly over the detector in the figure. Coregistration is achieved along scan for all bands by buffering the samples and time shifting them such that the reported samples will be coregistered along-scan for all bands The four FPAs are spatially coregistrated in the along track direction, but they are shown spread out in the figure for clarity. Also, band 32 has all of its detector laid out in the figure to show typical relative positions of the detectors within a band.

The spatial location accuracy of the MODIS ground footprint has two aspects: (1) the accuracy of the geolocation for a single reference band, and (2) the accuracy of the shift of other bands relative to the reference band. The geolocation for a single reference band will be provided by SDST and its accuracy will be improved during the A&E phase by removing biases. The SRCA will measure the MODIS detector position shift both along-scan and along-track on-orbit to determine the relative position of the MODIS bands/channels.

Pre-launch, GSE measures the MODIS relative detector positions along scan and along track of each MODIS detector. Based upon the measured relative detector position data the band-to-band percent registration will be determined prelaunch and compared with the specification. The GSE measurement resolution of the relative detector position is expected to be 1/40 of the detector size. Nearly at the same time when the GSE makes relative position measurements, the SRCA will measure the relative position along-scan for each detector and only the centroid position along-track for each band.

The detector (band) relative position measured by GSE and by the SRCA in TV may differ slightly due to the SRCA partial aperture filling. Correction values for the difference will be measured prelaunch. The SRCA measures the relative detector (band)

shift on-orbit. From prelaunch to on-orbit there could be relative shifts between the focal planes along scan and along track but the relative shifts between detectors within a focal plane should be negligible. The relative position difference measured by the SRCA between the prelaunch and on-orbit gives the detector (band) shifts. After correction for the GSE/SRCA bias measured prelaunch the on-orbit detector(band) positions are determined. On-orbit registration may be computed to check for specification compliance.

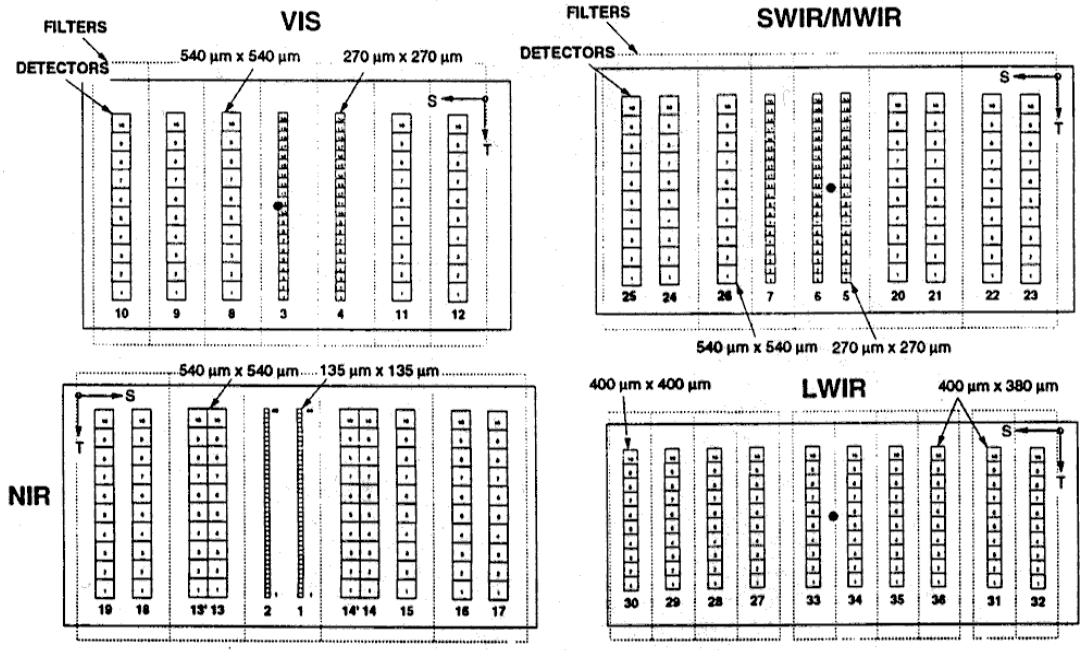

Figure 5.1.1 MODIS FPA detector geometry

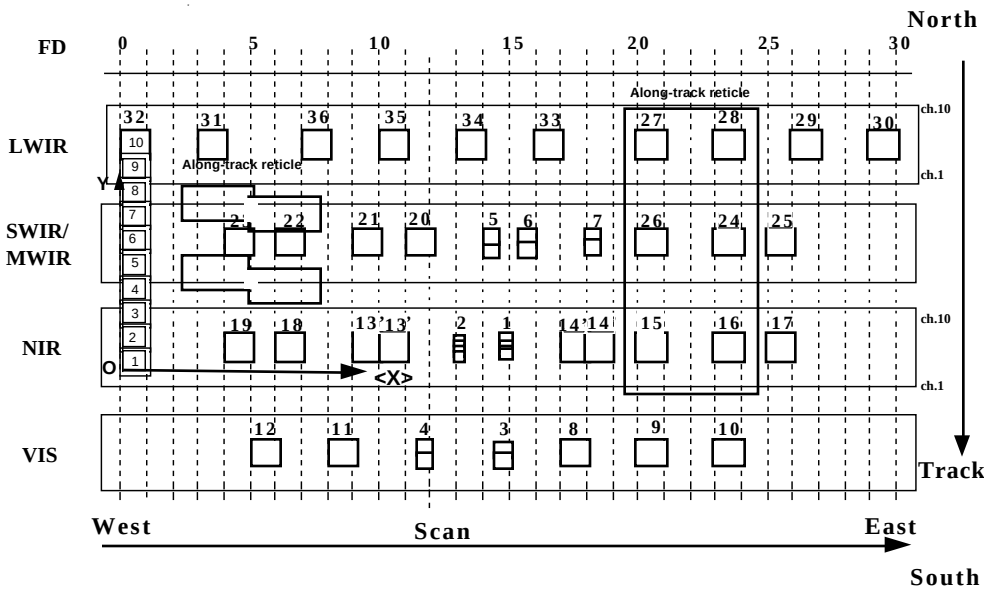

Figure 5.1.2 Co-registration of the bands in along-scan direction

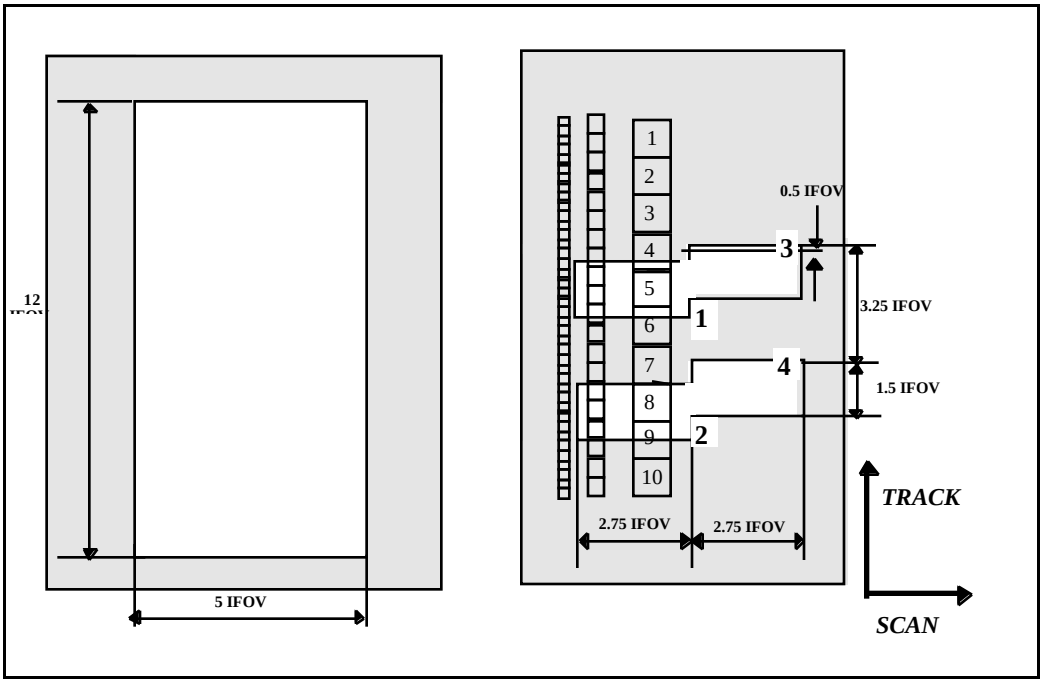

Figure 5.1.3 SRCA reticle patterns for spatial calibration

When the SRCA is in the spatial mode, the SRCA IR source, which is a heat resistance, is

powered to 390K ± 5K. Four SIS lamp configurations are used: 3-10W, 2-10W, 1-10W and 1-1W. A diachronic beam combiner in the filter wheel is selected, which combines the VIS/NIR /SWIR beam from the SRCA SIS with the IR beam from the thermal source. The spatial calibration covers most of the MODIS bands. If two or three bands are saturated the position for these bands can be determined by interpolation based upon the GSE measurement results.

In the monochromator portion of the SRCA (See Figure 2.1), the plain mirror is in position. The monochromator becomes a relay collimator. As various lamp combinations are introduced, the reticle motor alternately locates the along-scan reticle (5 × 1 km IFOV in the along-scan direction and 12 × 1 km IFOV in the along-track direction) and the along-track reticle (See Figure 5.1.3) into the optical path. The reticles, illuminated by the light sources, are imaged onto the MODIS focal planes. The reticle images are scanned across the MODIS detectors as the MODIS mirror rotates.

When the spatial calibration is for along-scan, the signals are sampled at a number of frames for each of a set of electronic sampling phase-delay settings. Those signals are sampled when the leading edge and the trailing edge of the along-scan reticle are located at a variety of known positions relative to the detectors for all bands. The signals provide the data for determining the relative position and shifts of the detectors (bands) on-orbit.

The along-track reticle is unique in shape (See Figure 5.1.3). There are four square openings. The four openings have a size of 2.75 IFOV (1 km) in along-scan direction and 1.5 IFOV (1 km) in along-track direction. The two right openings, marked as 3 and 4, are shifted up by 0.5 IFOV (1 km) relative to the two left openings, marked as 1 and 2, and the two upper opening are shifted from the two lower openings by 3.25 IFOV (1 km). Thus, multi-detector can be partially or fully opened or shaded by the four apertures. Processing of these data allows determination of the centroid position shift along track of a band.

5.2 Implementation of spatial calibration

When the SRCA is in spatial mode, a single 10W lamp and the IR source will be turned on to verify whether the SRCA is properly configured. The verification includes a check of lamp current, voltage, detector signals, the IR source current and temperature.

The spatial calibration is implemented by stepping down through the following four lamp configuration: 3-10W, 2-10W, 1-10W, and 1-1W while the IR source is on. In the same way as in the radiometric calibration, the 2-10W lamp configuration uses different lamps from the 1-10W lamp configuration for saving the life of the 1-10W lamp. The along-scan and along-track reticles will be alternately flipped into the optical path.

The reticle can be treated as a bright target on the ground because the reticle is placed at the focal plane of the SRCA collimator. When the scan mirror rotates, the detector footprint scans across the reticle and generates the calibration signals. The projected reticle is also drawn in Figure 5.1.2 for understanding the relative positioning purpose. However, the position of the projected reticle is randomly drawn in along-scan direction because the data from each detector is lined-up and it does not matter where the projected reticle is drawn in the along-scan direction.

The number of frames of Earth View data is 1354 for all Bands 1-36. There are three different types of frames of data corresponding to the 3 different IFOVs (0.25 km, 0.5 km, and 1.0 km resolution detectors). The 0.25 km, 0.5 km and 1.0 km bands have 4×1354 samples, 2×1354 and 1×1354 samples for each scan across the earth. SBRS defines a "frame" to be the data covering a 1-km IFOV. This leads to a natural indexing arrangement for all 36 Bands (frame, sub-sample per frame) with frame going from 1-1354, and sub-sample per frame (SSPF) going from 1-4 for bands 1-2, 1-2 for bands 3-7 and 1-1 for bands 8-36. This applies appropriately to all bands.

When the SRCA is in spatial mode, the output data for all bands are co-registered (lined-up). Ten effective frames of data are collected for each band. Similar to the case in earth viewing, the 0.25 km, 0.5 km, and 1.0 km bands have 40, 20, and 10 samples collected respectively when the SRCA reticle is being scanned.

The operational orders of along-scan and along-track are reversed when the lamp configuration changes to minimize reticle motion. The procedure and the corresponding bands to be calibrated are listed in Table 5.2.1.

In the Table 5.2.1, $\boldsymbol{N_{sample}}$ is the effective numbers of samples in spatial calibration. Since the reticle has a width of five IFOVs (1 km), the maximum number of frames of data (1 frame of data equals to 1 km IFOV in size) is seven. Including some margins on both sides, $\boldsymbol{N_{frame}}$ is set to ten, corresponding 40 samples for 0.25 IFOV bands, 20 samples for 0.5 IFOV bands, and 10 samples for 1 km IFOV bands). $\boldsymbol{N_{phase}}$ is the number of phase-delays. This number equals to six and is the same for all detectors. The phase-delay setting is 0.0 IFOV, 0.2 IFOV, 0.4 IFOV, 0.6 IFOV, 0.8 IFOV, and 1.0 IFOV. The phase-delay setting of 1.0 IFOV should have the same signal as phase-delay setting of 0.0 IFOV for the next frame number. This provides a consistence checking. However, the data for the phase-delay of 1.0 IFOV is skipped in the calculation of the centroid position and its shift.

Table 5.2.1 Implementation procedure of the spatial calibration using the SRCA

No.	Lamp configuration	Reticle pattern	Number of sampling (Sample × phase-delay)	Band to be calibrated
1	3-10W	along-scan	$\boldsymbol{N_{sample} \times N_{phase}}$	3, 8, 9

	IR source	along-scan	$N_{sample} \times N_{phase}$	20-25, 27-36
2	3-10W	along-track	N_{sample}	3, 8, 9
	IR source	along-track	N_{sample}	20-25, 27-36
3	2-10W	along-track	N_{sample}	1, 4, 10
4	2-10W	along-scan	$N_{sample} \times N_{phase}$	1, 4, 10
5	1-10W	along-scan	$N_{sample} \times N_{phase}$	2, 11
6	1-10W	along-track	N_{sample}	2, 11
7	1-1W	along-track	N_{sample}	5-7, 12-19, 26
8	1-1W	along-scan	$N_{sample} \times N_{phase}$	5-7, 12-19, 26

5.3 Mathematical description of the algorithm to determine the relative position of each MODIS detector in the along-scan direction:

Data will be collected for a number of scans, N_{scan}, for two mirror sides, N_{side}=2, for an effective number of samples, $N_{sample,}$, and for a number of phase-delays, N_{phase} , for each MODIS band/detector.

The DN values are pre-corrected for space count bias, scan angle effect, detector non-linearity, temperature effect of the detector response and mirror reflectivity (as a function of mirror side and scan angle). However, the signals for each mirror side must be processed separately due to possible un-parallel mirror sides in the along-scan direction.

5.3.1 Determine Aperture Response Function along-Scan (ARFS)

The data average over number of scans for each sample, phase-delay setting, and mirror side for each detector is called the Aperture Response Function along-Scan (ARFS).

$$ARFS_{b,ch}(sample\#, phase\#, side\#) = \frac{\sum_{i=1}^{N_{scan}} DN_{b,ch}(scan\#, sample\#, phase\#, side\#)}{N_{scan}} \qquad (5.3.1)$$

where subscript ***b*** is band number, ***ch*** is the channel number; ***sample#*** is sample number (1-40 for bands 1 and 2; 1-20 for bands 3-7; 1-10 for bands 8-36); ***frame#*** is the effective frame number which is from 1 to10 for all bands. N_{SSPF} is the number of sub-sample per frame. ***SSPF#*** is sub-sample per frame number. ***phase#*** is the phase delay setting number from 0-5 corresponding to phase-delay setting of 0 , 0.2, 0.4, 0.6, and 0.8 IFOV, ***scan#*** is the scan number, ***side#*** is the mirror side number, and N_{scan} is the number of scans for averaging. The relationship between ***sample#*** and ***frame#*** and ***SSPF#*** is

$$sample\# = (frame\# - 1) \cdot N_{SSPF} + SSPF\#$$

5.3.2. Determine the Combined ARFS (CARFS).

The CARFS is the combined or interlaced data values for all the frames and phase-delays according to the location of the sample on the FPAs.

Define $\boldsymbol{X}$ as

$$\boldsymbol{X = FD + (sample\# \cdot sample\_size - 1) + delay\# \cdot phase\_length} \qquad (5.3.2)$$

FD (km) is the nominal location along scan of a detector in band b relative to the left edge of band 32. X (IFOV) is the nominal location along scan of sample # of band b relative to the left edge of band 32 at its 1st sample (See Figure 5.1.2 and Table 5.3.1). The ***sample_size*** is one (1-km IFOV), half (0.5-km IFOV), or quarter (0.25-km IFOV). The ***delay#*** is zero to four and the phase-delay length, ***phase_length***, is 0.2.

When the detectors take samples, the signal, called Combined Aperture Response Function along-Scan, for band# of b, channel# of ch, and mirror side of side# is

$$\boldsymbol{CARFS_{b,ch}(X, side\#) = ARFS_{b,ch}(sample\#, phase\#, side\#)} \qquad (5.3.3)$$

A CARFS curve is shown in Figure 5.3.1.

5.3.3. Calculate the spatial center value for each MODIS detector

The first moment of $\boldsymbol{CARFS_{b,ch}}$ gives the spatial centroid position of a detector.

$$\boldsymbol{< X >_{b,ch,side} = size \cdot \left[\frac{\sum_{N_{frame}} CARFS_{b,ch}(X, side\#) \cdot X}{\sum_{N_{frame}} CARFS_{b,ch}(X, side\#)} - PST_{b,S} \right]} \qquad (5.3.4)$$

where ***IFOV*** is IFOV value (km). $\boldsymbol{PST_b}$ is the frame number that the center position is away from its edge to count frame along-scan (2.625 for 0.25 km IFOV bands, 2.75 for 0.5 km IFOV bands, 3.0 for 1 km IFOV bands). The $\langle \boldsymbol{X} \rangle$ is the relative positions of detectors within their focal plane arrays (FPAs).

Table 5.3.1 shows the relationship between number of sample, X value, and $\langle \boldsymbol{X} \rangle$ value during SRCA operation for all 36 MODIS bands, including the 2 pairs of time delay integration (TDI) bands 13', 13 and 14',14.

Suppose that a detector is shifted towards FD decreasing direction. In that circumstance, the signal will increase for the same X value for the left part of the CARF and decrease for the right part of the CARF because the aperture opens a greater/smaller area for that detector. the CARFS curve shifts towards -X direction as showing in Figure 5.3.1 in result of smaller $\langle \boldsymbol{X} \rangle$. Comparing to prelaunch $\langle \boldsymbol{X} \rangle$, a shift of $\langle \boldsymbol{X} \rangle$ is given which indicates the real position shift in the its FPA.

Table 5.3.1. X value and number of samples for SRCA data

Band	Resolution (km)	Number of Sample	FD value*	X value (start)	X value (end)
1	0.25	40	14.875	14.875	24.675
2	0.25	40	13.125	13.125	22.925
3	0.5	20	14.75	14.75	24.55
4	0.5	20	11.75	11.75	21.55
5	0.5	20	14.25	14.25	24.05
6	0.5	20	15.75	15.75	25.55
7	0.5	20	18.25	18.25	28.05
8	1	10	17.5	17.5	27.3
9	1	10	20.5	20.5	30.3
10	1	10	23.5	23.5	33.3
11	1	10	8.5	8.5	18.3
12	1	10	5.5	5.5	15.3
13	1	10	10.5	10.5	20.3
13’	1	10	9.5	9.5	19.3
14	1	10	18.5	18.5	28.3
14’	1	10	17.5	17.5	27.3
15	1	10	20.5	20.5	30.3
16	1	10	23.5	23.5	33.3
17	1	10	25.5	25.5	35.3
18	1	10	6.5	6.5	16.3
19	1	10	4.5	4.5	14.3
20	1	10	11.5	11.5	21.3
21	1	10	9.5	9.5	19.3
22	1	10	6.5	6.5	16.3
23	1	10	4.5	4.5	14.3
24	1	10	23.5	23.5	33.3
25	1	10	25.5	25.5	35.3
26	1	10	20.5	20.5	30.3
27	1	10	20.5	20.5	30.3
28	1	10	23.5	23.5	33.3
29	1	10	26.5	26.5	36.3
30	1	10	29.5	29.5	39.3
31	1	10	3.5	3.5	13.3
32	1	10	0.5	0.5	10.3
33	1	10	16.5	16.5	26.3
34	1	10	13.5	13.5	23.3
35	1	10	10.5	10.5	20.3
36	1	10	7.5	7.5	17.3

Note*: In ideal detector layout situation. The value is counted from the center of the detector, the <X> value equals to FD value for the first frame and zero phase-delay.

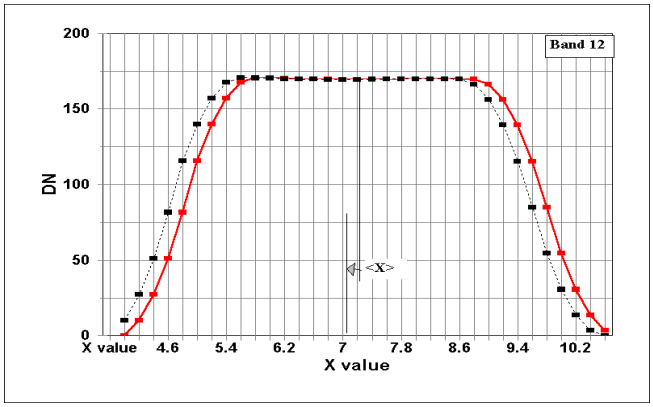

Figure 5.3.1 CARFS(X) profile

5.3.4 Calculate the MODIS detector shift along-scan

The detector shift is the difference between the spatial centriod position of the detector on-orbit, $\langle X \rangle_{b,ch}$, and that prelaunch, $\langle X \rangle_{b,ch,o}$. The detector shift is averaged over mirror sides.

$$\langle \Delta X \rangle_{b,ch} = \frac{(\langle X \rangle_{b,ch,1} - \langle X \rangle_{b,ch,o,1}) + (\langle X \rangle_{b,ch,2} - \langle X \rangle_{b,ch,o,2})}{2} \qquad (5.3.5)$$

The $\langle X \rangle_{b,ch}$ is positive if the detector shifts towards the scan direction.

We notice that the effect of unparalleled mirror sides has been avoided in determining the shift between prelaunch and on-orbit.

5.3.5 Calculate the current detector position along-scan

The prelaunch spatial position difference, $\langle \Delta X \rangle_{b,ch,o}$, measured by the GSE and the SRCA is

$$\langle \Delta X \rangle_{b,ch,o} = \frac{(\langle X \rangle_{b,ch,o,1,GSE} - \langle X \rangle_{b,ch,o,1,SRCA}) + (\langle X \rangle_{b,ch,o,2,GSE} - \langle X \rangle_{b,ch,o,2,SRCA})}{2} \qquad (5.3.6)$$

The current on-orbit detector position along-scan is

$$\langle X \rangle_{b,ch} = \langle X \rangle_{b,ch,o} + \langle \Delta X \rangle_{b,ch} + \langle \Delta X \rangle_{b,ch,o} \qquad (5.3.7)$$

5.4. Mathematical description of the algorithm to determine centroid position for each MODIS band in the along-track direction

For along-track spatial calibration data collection is the same as that for along-scan except that there is no phase-delay change for the along-track direction.

The signals for each mirror side must be separately processed due to possible un-parallel mirror sides in along-track direction.

A feature of the along-track algorithm is the introduction of spatial coordinate transformations for each of the four openings. These transformations cause the signals through the four apertures to coincide spatially in such a way to determine the centroid value. We will detail that in the algorithm.

When the image of the along-track reticle scans across the detectors, some of the detectors will be fully illuminated , some will be partially illuminated, while the rest will be totally dark (covered) (See Figure 5.1.3). Unlike the along-scan situation, the along-track has only a single fixed phase-delay for each Focal Plane Assembly (FPA). That means there will be only one data sample per frame position. The phase delay will be adjusted such that the seven to eight effective samples (for 1 km IFOV) will be symmetrical with respect to data coverage about the reticle centerline.

Using the entire set of samples to determine the centroid position along-track, a method similar to the Aperture Response Function along-Scan, is not appropriate because of the limited data set, especially for the 1-km IFOV case. Instead only one data sample be used for each of the four apertures. The band centroid position along-track is determined by all detector signals of a band weighted by the edge positions along-track, $\boldsymbol{Y_{b,ch}}$.

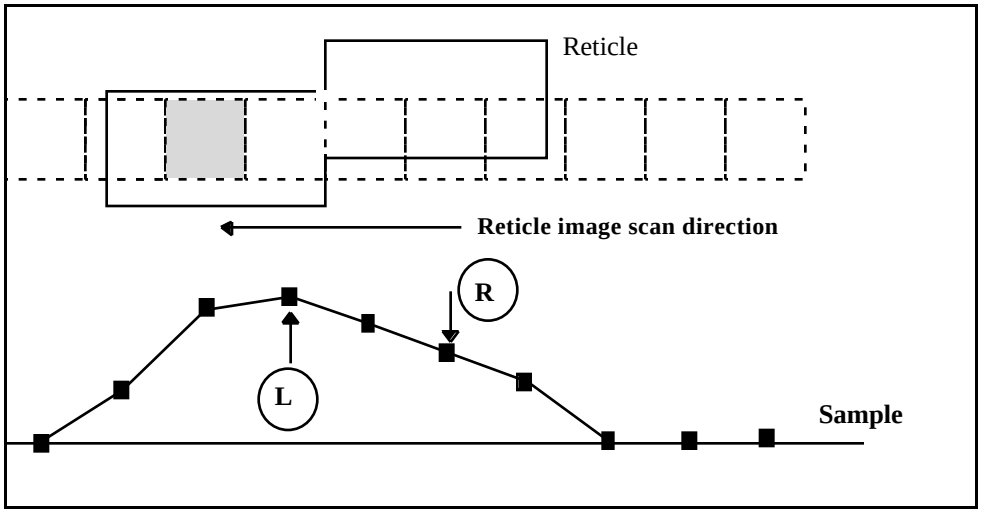

Figure 5.4.1 DN value in one scan of the along-track reticle

The single sample data used in calculation of the centroid position must correspond to a reticle position such that the reticle is located where the detector is fully illuminated in along-scan direction (not necessary in along-track direction) and the detector has a "stable" signal. A "stable" signal is defined such that the electronic integrator is not in signal transitional stage but at a "stable" stage. The photon flux upon the detector does not change during the integration period for a "stable" sample. As an example, Figure 5.4.1 shows the signals for a single detector (1-km IFOV) as a function of sample number. In the figure the arrow marked "L" is the sample fully illuminated through the left aperture and is expected to have a "stable" DN and the arrow marked "R" is the same but illuminated through the right aperture. The two DNs are the data points utilized for determining the band centroid position along-track for that detector.

5.4.1 Using the MODIS along-scan response to correct the non-uniform output of the SRCA

A flat fielding correction must be utilized as a preprocess to eliminate the effect of non-uniformity of MODIS channel responses to the SRCA output on the band centroid value. The correction requires the MODIS DN values, when illuminated by the SRCA with the along-scan reticle in place. The algorithm is as follows:

5.4.1.1. Find the average DN, $DN_{SRCA,max}(b,ch)$, of three highest DN values over a scan for each channel. The methodology is the same as in radiometric calibration where the average DN is determined.

5.4.1.2. Calculate the average value of $DN_{SRCA,max}(b,ch)$ over a band

$$DN_{SRCA,av}(b) = \frac{1}{N_{ch}(b)} \sum_{ch=1}^{N_{ch}(b)} DN_{SRCA,max}(b,ch) \qquad (5.4.1)$$

5.4.1.3. In order to zero-out the weight due to the non-uniform response of MODIS channel/band to the SRCA, the correction coefficient is

$$C_{SRCA}(b,ch) = \frac{DN_{SRCA,av}(b)}{DN_{SRCA,max}(b,ch)} \qquad (5.4.2)$$

5.4.1.4. For any DN in along-track calibration, the corrected DN is

$$DN_{SRCA}(b,ch) = C_{SRCA}(b,ch) \cdot DN_{SRCA}(b,ch) \qquad (5.4.3)$$

5.4.2. Average DN over number of scans:

$$DN_{b,ch}(ds,side) = \frac{1}{N_{scan}} \sum_{scan=1}^{N_{scan}} DN_{b,ch}(scan,ds,side) \qquad (5.4.4)$$

where ***ds*** is sample number and ***side*** is scan mirror side number.

5.4.3. Find the maximum $DN_{b,ch,max}(side)$ over the effective number of scans

If $DN_{b,ch,max}(side)$ is less than dark DN plus three times the expected noise DN_{noise}, $DN_{b,ch,dark}+3(DN_{noise})$, that means this channel is not illuminated through the reticle aperture. We set $DN_{b,ch,L}(side)$ and $DN_{b,ch,R}(side)$ to zero and jump over to the next step, 5.4.4.

5.4.4. Pick up two sample DNs.

The two samples are located at the full open position by the left and right apertures respectively and "stable" DNs are achievable. The strategy for determining the two samples, $DN_{b,ch,L}$ and $DN_{b,ch,R}$, differs depending upon detector size.

5.4.4.1 For bands of 1km IFOV

5.4.4.1.1. Find the maximum DN for each detector over ten effective sample numbers (sample position, see Figure 5.4.1). The corresponding sample number is named df_{max}. The first effective sample number starts one frame before the reticle begins to illuminate this band. The DN of the sample number df_{max} serves as the first data point for that detector while the second data sample is located two or three samples away from the df_{max}.

5.4.4.1.2. Determine the number of frames which separate one data point from the other for a designated band.

5.4.4.1.2.1. Calculate the maximum DN over frames and channels, $DN_{max}(b)$.

5.4.4.1.2.2. Count the frequency of the frame numbers for which the DN is greater than $0.4\times DN_{max}(b)$.

5.4.4.1.2.3. The separation of the two frame numbers with highest frequency is named ***cnt100***.

5.4.4.1.3. In order to determine whether the second data sample is located on the left or on the right side of the df_{max} we compare the DNs for the sample number df_{max}-3 and df_{max}+3. Since one of them must be fully covered by the reticle (no light), the sample number with greater DN, corresponding to the second data point, is selected and named df_{cmp} (complementary to df_{max}).

5.4.4.1.4. If $df_{cmp} < df_{max}$: Then the data sample value, when the detector is illuminated through the left aperture, $DN_{b,ch,L}(side)$, equals to $DN_{b,ch}(df_{max}$-

cnt100,side); and the data sample value, when the detector is illuminated through the right aperture, $DN_{b,ch,R}(side)$, is equal to $DN_{b,ch}(df_{max},side)$.

In contrast, if $df_{cmp} > df_{max}$, $DN_{b,ch,L}(side) = DN_{b,ch}(df_{max},side)$ and $DN_{b,ch,R}(side) = DN_{b,ch}(df_{max}+cnt100,side)$.

The flowchart is shown in Figure 5.4.2 (for simplicity, "side" has been omitted in the DN expression, it is also omitted in the following flowchart).

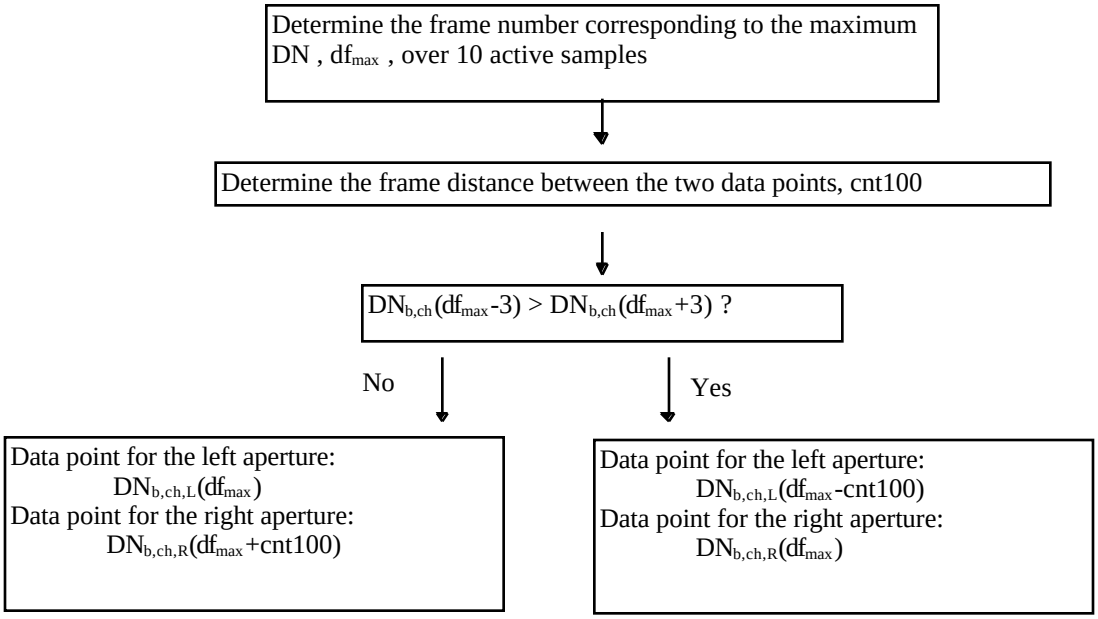

Figure 5.4.2. The flowchart for picking up data point pair for a typical scan (1- km IFOV case)

5.4.4.2 For bands of 0.5 km IFOV

For the 0.5 km IFOV the number of data samples is doubled comparing to 1-km IFOV case. If during a scan a detector is illuminated through one of the apertures in the reticle then there are at least three samples which are fully illuminated through the left and another three samples which are illuminated through the right apertures with "stable" DNs. The algorithm will determine the location of the left three samples and the right three samples. Then the average of one of the sets of three DNs give the $DN_{b,ch,L}(side)$ and the average of the other set of three DNs gives the $DN_{b,ch,R}(side)$.

The method of determining two sets of three-fully-illuminated samples is to compare the sums of the two standard deviations. If the sum of the standard deviation of the two DNs corresponding to the two three-fully-illuminated samples is minimum, we

can say that the $DN_{b,ch,L}(side)$ and $DN_{b,ch,R}(side)$) are what we need for the calculation of the band centroid position. The procedures are as follows:

5.4.4.2.1. Find the maximum DN for each detector over twenty effective sample numbers. The corresponding frame number is df_{max}.

5.4.4.2.2. Pick up five sequential data samples, from $df_{max}-2$ to $df_{max}+2$.

5.4.4.2.3. Calculate the standard deviations for three groups of data:

$$\sigma_I = std\left[DN_{b,ch}\,(df_{max} + I + J, side), J = -3 \text{ to } -1 \right], \text{where } I=1,3 \qquad (5.4.5)$$

Notice that df_{max} must be one of the data in each data group.

5.4.4.2.4. Find the group number, I_{av}, with the minimum standard deviation among the three σs. The average sample number, df_{av}, of the three equals to df_{av}. The reason for calculating the average sample number is to determine whether a group of data belongs to the left aperture or to the right aperture.

5.4.4.2.5 Notice in Figure 5.1.3 that the detector number 16 is fully illuminated through the along-track reticle. We need to find the sample number which divides the left aperture and right aperture.

- Find the maximum $DN_{b,ch}(df,side)$, $DN_{b,ch,max}(side)$, over number of samples for the selected channel.

- Pick up all sample numbers with DNs greater than $0.3\times DN_{b,ch,max}(side)$. The average of these sample numbers is the center and is named $df_{b,ch,ctr}(side)$. The default value is 9.

5.4.4.2.6. If df_{av} is greater than $df_{b,ch,ctr}(side)$, the sample df_{av} is illuminated through the right aperture; otherwise, the sample df_{av} is illuminated through the left aperture.

The second group of standard deviations, six samples away from the sample number in 5.4.4.2.3, needs to be calculated.

If $df_{av} > df_{b,ch,ctr}(side)$:

$$\sigma'_I = std\left[DN_{b,ch}\,(df_{max} + I + J, side), J = -8 \text{ to } -6) \right], \text{ where } I=1,3 \qquad (5.4.6)$$

If $df_{av} < df_{,ch,ctr}(side)$:

$$\sigma'_I = std\left[DN_{b,ch}(df_{max} + I + J, side), J = 2to\ 4)\right], \text{ where } I=1,3 \quad (5.4.7)$$

5.4.4.2.7. Calculate the sum of three groups of standard deviations

$$\sigma_{sum,I} = \sigma_I + \sigma'_I \quad (5.4.8)$$

5.4.4.2.8. Find the value I for which $\sigma_{sum,I}$ (I=1,3) is minimum and call it I_{GP}.

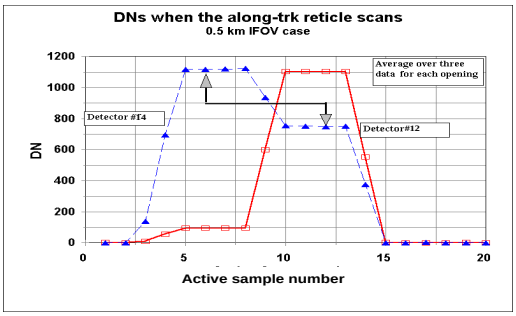

The initial data sample for which DN is to be included in the average is

$$df_{ini}=df_{av}+I_{GP}-4 \quad (5.4.9)$$

Figure 5.4.3. DNs as a function of effective sample number for two typical detectors of 0.5 km IFOV

5.4.4.2.9. The two DN values for the data points needed are

If $df_{av} < df_{b,ch,ctr}(side)$:

$$DN_{b,ch,L}(side) = \frac{1}{3}\sum_{K=0}^{2} DN_{b,ch}(df_{ini} + k, side) \quad (5.4.10)$$

$$DN_{b,ch,R}(side) = \frac{1}{3}\sum_{K=0}^{2} DN_{b,ch}(df_{ini} + k + 5, side) \quad (5.4.11)$$

If $df_{av} > df_{b,ch,ctr}(side)$:

$$DN_{b,ch,L}(side) = \frac{1}{3}\sum_{K=0}^{2} DN_{b,ch}(df_{ini} + k - 5, side) \quad (5.4.12)$$

$$DN_{b,ch,L}(side) = \frac{1}{3}\sum_{K=0}^{2} DN_{b,ch}(df_{ini} + k, side) \quad (5.4.13)$$

Figure 5.4.3 shows the DNs as a function of effective sample number as the along-track reticle scans across a detector. The flow chart for determining the data pair is shown in Figure 5.4.4.

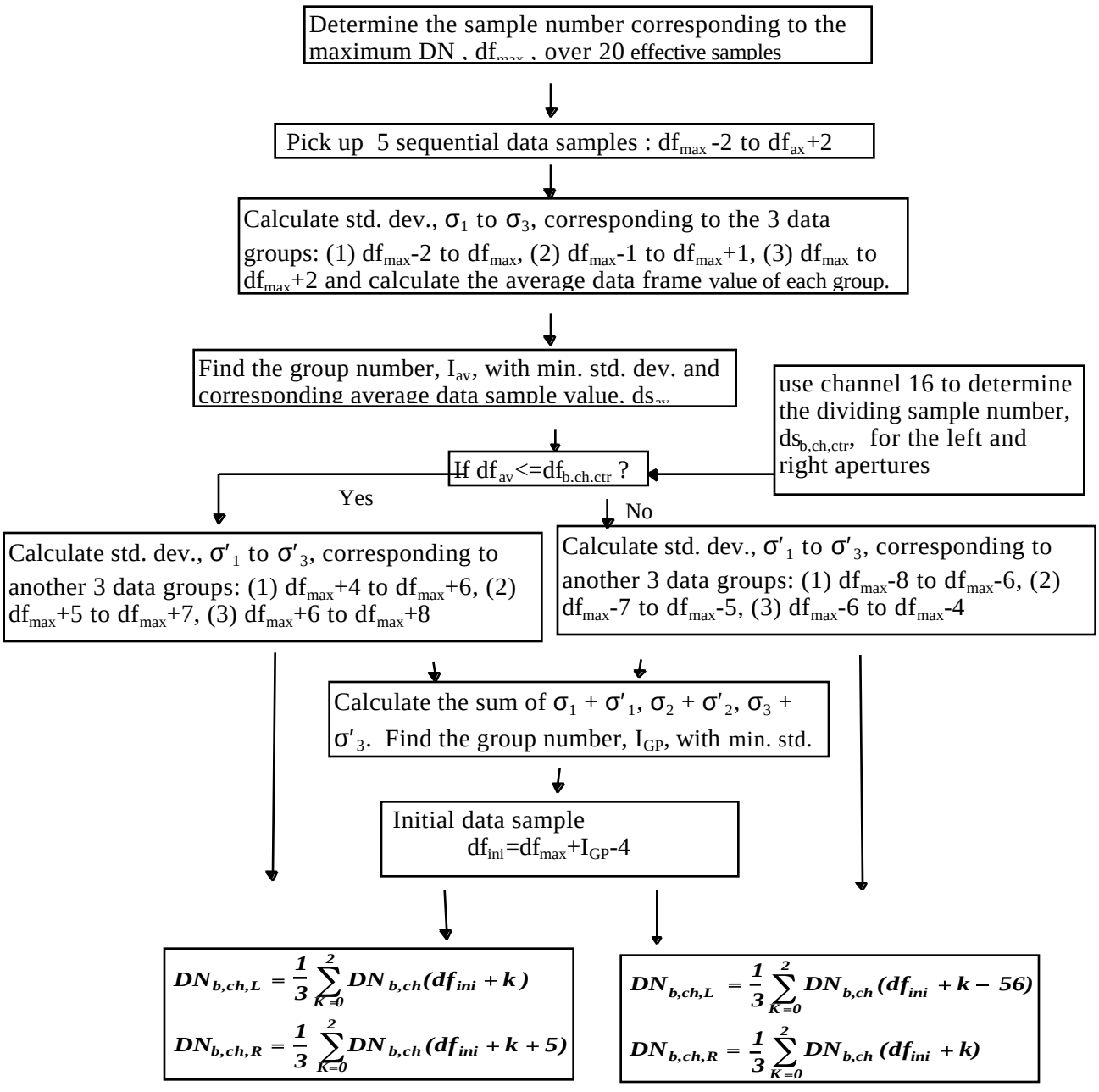

Figure 5.4.4. The flow chart of determining data pair (0.5 km case)

5.4.4.3 For bands of 0.25 km IFOV

The methodology is the same as for the 0.5 km IFOV case except the number of samples for averaging. If during a scan a detector is illuminated through one of the apertures in the reticle then there exists at least eight fully illuminated samples for each aperture. Considering the possible FPA rotation and magnification change, we average six fully illuminated samples for each aperture. The procedures are listed as follows:

5.4.4.3.1. Find the maximum ***DN*** for each detector over forty effective sample numbers. The corresponding sample number is df_{max}.

5.4.4.3.2. Pick up eleven sequential data samples, from df_{max}-5 to df_{max}+5.

5.4.4.3.3. Calculate the standard deviations of six groups of data:

$$\sigma_I = std\left[DN_{b,ch}(df_{max} + I + J, side), J = -6 \text{ to } -1) \right], \text{where } I=1,6 \qquad (5.4.14)$$

5.4.4.3.4. Find the group number, I_{av}, with the minimum standard deviation of the six σs. This averaged sample number, df_{av}, of the six rounds up to the integer df_{max}-4+I_{av}.

5.4.4.3.5. Notice that there are more detectors which are fully illuminated through the along-track reticle (left and right apertures). In order to find the sample numbers corresponding to the dividing line of the left and right apertures, only one of these channels is used. We use detector 30. The method is the same as for 0.5 km IFOV case.

- ♦ Find the maximum $DN_{b,ch}(df,side)$, $DN_{b,ch,max}(side)$, over number of effective samples for the selected detector.

- ♦ Pick up all sample numbers with DNs greater than $0.3 \times DN_{b,ch,max}(side)$. The average of these sample numbers is named $df_{b,ch,ctr}(side)$. The default value is 18.

5.4.4.3.6. If df_{av} is greater than $df_{b,ch,ctr}(side)$, the sample df_{av} is illuminated through the right aperture; otherwise, the sample df_{av} is illuminated through the left aperture. The second group of standard deviations, eleven samples away from the sample number in 5.4.4.3.3, needs to be calculated.

If $df_{av} > df_{b,ch,ctr}(side)$:

$$\sigma'_I = std\left[DN_{b,ch}(df_{max} + I + J, side), J = -17 \text{ to } -12) \right], \text{ where } I=1,6 \qquad (5.4.15)$$

If $df_{av} < df_{,ch,ctr}(side)$:

$$\sigma'_{I} = std\left[DN_{b,ch}(df_{max} + I + J, side), J = 5 \text{ to } 10) \right] \text{where } I=1,6 \quad (5.4.16)$$

5.4.4.3.7. Calculate the sum of six groups of standard deviations

$$\sigma_{sum,I} = \sigma_{I} + \sigma'_{I} \quad (5.4.17)$$

5.4.4.3.8. Find the value I for which $\sigma_{sum,I}$ $(I=1,6)$ is minimum and call it I_{GP}. The initial data sample number is $ds_{ini}=ds_{max}+I_{GP}-7$.

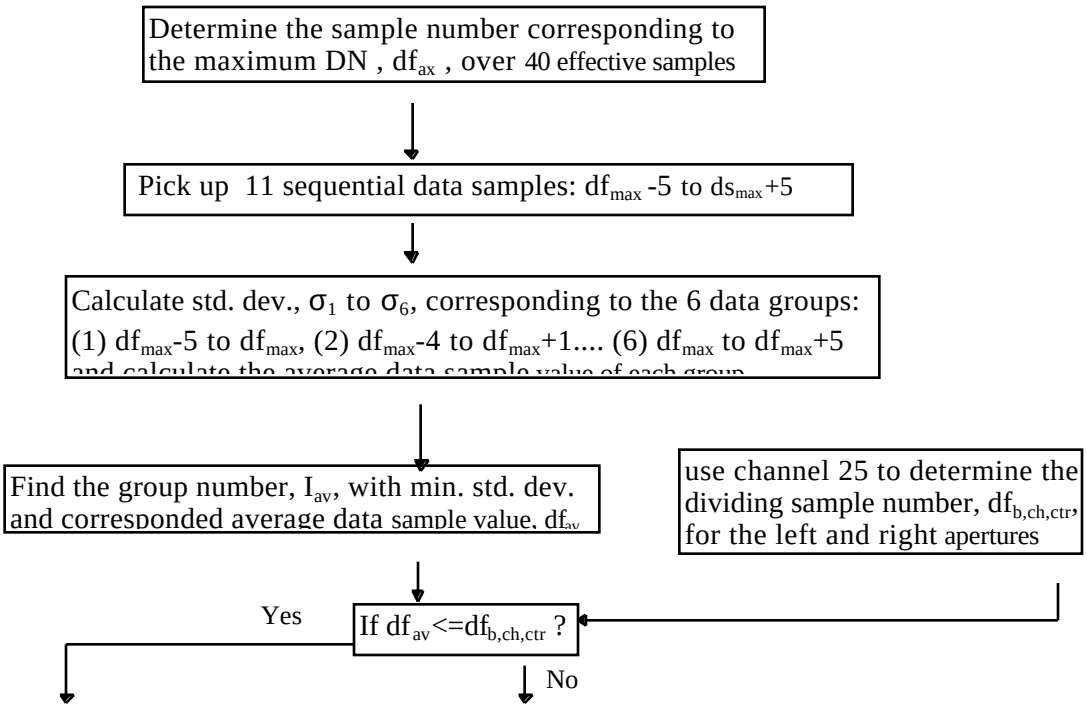

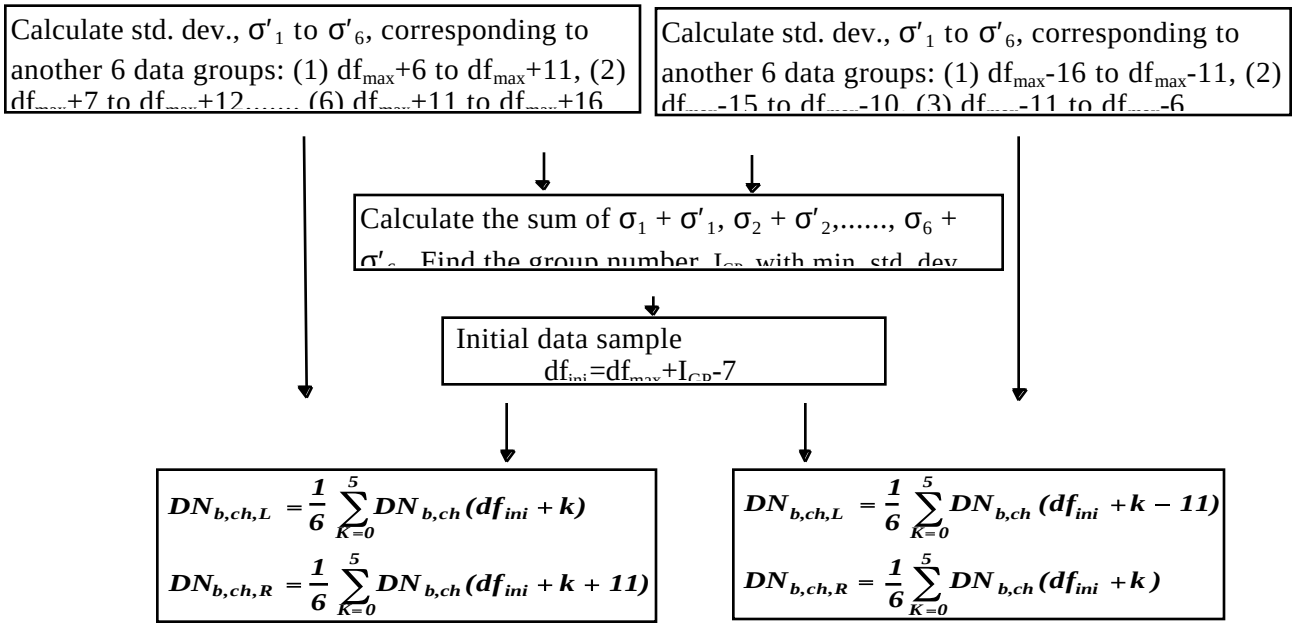

Figure 5.4.5. The flowchart of determining data pair (0.25 km IFOV case)

(9) The two DN values for the data points needed are

If $df_{av} < df_{b,ch,ctr}(side)$:

$$DN_{b,ch,L}(side) = \frac{1}{6}\sum_{K=0}^{5} DN_{b,ch}(df_{ini} + k, side) \quad (5.4.18)$$

$$DN_{b,ch,R}(side) = \frac{1}{6}\sum_{K=0}^{5} DN_{b,ch}(df_{ini} + k + 11, side) \quad (5.4.19)$$

If $df_{av} > df_{b,ch,ctr}(side)$:

$$DN_{b,ch,L}(side) = \frac{1}{6}\sum_{K=0}^{5} DN_{b,ch}(df_{ini} + k - 11, side) \quad (5.4.20)$$

$$DN_{b,ch,L}(side) = \frac{1}{6}\sum_{K=0}^{5} DN_{b,ch}(df_{ini} + k, side) \quad (5.4.21)$$

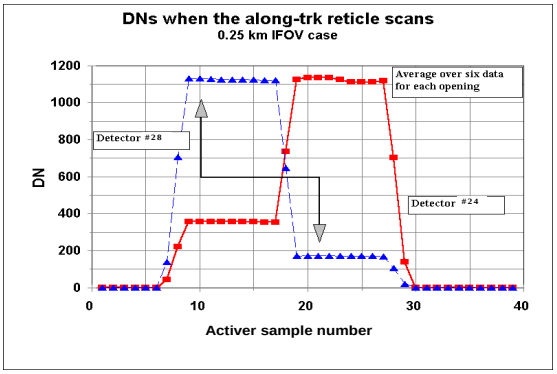

Figure 5.4.6. DNs as a function of effective sample number for two detectors of 0.25 km IFOV

Figure 5.4.5 is the flowchart for determining the data pair for the 0.25 km IFOV case. Figure 5.4.6 shows DNs as a function of effective sample number when the along-track reticle scans across two detectors of 0.25 km IFOV.

5.4.5. Determination of the weighted phase position for each detector, $Y_{b,ch}$

Table 5.4.1 shows the detector / aperture combination for each of the four apertures. The table also gives a coordinate transformation associated with the distance between the four apertures. The transformation, expressed as $\boldsymbol{Y_{b,ch}}$, causes the centroid of the four apertures to coincide.

Table 5.4.1. $\boldsymbol{Y_{b,ch}}$ values

	Left aperture	Right aperture
Detectors from 1 to 6/IFOV	aperture 1: $\boldsymbol{Y_{b,ch,L}}$ = ch · IFOV	aperture 1: $\boldsymbol{Y_{b,ch,R}}$ = ch · IFOV + 0.50
Detectors from 1+6/IFOV to 10/IFOV	aperture 1: $\boldsymbol{Y_{b,ch,L}}$ = ch · IFOV - 3.25	aperture 1: $\boldsymbol{Y_{b,ch,R}}$ = ch · IFOV - 2.75

where ch = channel number, IFOV = IFOV (km).

It should be noticed that the Y coordinates established here is in the opposite direction of along-track. The smaller the channel number, the lower the Y value.

When the band is shifted in along-track direction, the $\langle Y \rangle_b$ must have the same direction and value for that shift. Table 5.4.2 gives a simple example to show that the $\langle Y \rangle_b$ gives the real shift value along-track. In the table, the $Y_{b,ch}$ is calculated by Table 5.4.1. The data in column 3 is called dn which equals to 1 for simlicity if the detector is fully illuminated by the aperture. The data in column 5 is that the detector is shift along-track for 0.1 IFOV. In that circumstance the dn value changes. The last row is $\langle Y \rangle_b$ which is calculated by Eq. (5.4.22). The $\langle Y \rangle_b$ gives the real shift value of the band.

Table 5.4.2 An example showing the $\langle Y \rangle_b$ gives the real shift along-track

		Origin position		Shift along-track for 0.1 IFOV	
Channel	**$Y_{b,ch}$**	**dn**	**$Y_{b,ch}$•dn**	**dn**	**$Y_{b,ch}$•dn**
Left aperture					
1	1	0	0	0	0
2	2	0	0	0	0
3	3	0	0	0	0
4	4	0.5	2	0.4	1.6
5	5	1	5	1	5
6	6	0	0	0.1	0.6
7	3.75	0.25	0.9375	0.15	0.5625
8	4.75	1	4.75	1	4.75
9	5.75	0.25	1.4375	0.35	2.0125
10	6.75	0	0	0	0
Right aperture					
1	1.5	0	0	0	0
2	2.5	0	0	0	0
3	3.5	0	0	0	0
4	4.5	1	4.5	0.9	4.05
5	5.5	0.5	2.75	0.6	3.3
6	6.5	0	0	0	0
7	4.25	0.75	3.1875	0.65	2.7625
8	5.25	0.75	3.9375	0.85	4.4625
9	6.25	0	0	0	0
10	7.25	0	0	0	0
$<Y>_{b,ch}$			0		0.1

5.4.6 Determine the spatial centroid position along-track for each MODIS band

Introduction of the $Y_{b,ch}$ allows the spatial centroid value to be calculated in a way which is similar to the along-scan algorithm. The spatial centroid position along-track for each MODIS band is

$$\langle Y \rangle_{b,side} = \left\lceil \frac{\sum_{ch=1}^{N_{ch}} \left[DN_{b,ch,L}(side) \cdot Y_{b,ch,L} + DN_{b,ch,R}(side) \cdot Y_{b,ch,R} \right]}{\sum_{ch=1}^{N_{ch}} \left[DN_{b,ch,L}(side) + DN_{b,ch,R}(side) \right]} \right\rceil - PST_{b,T} \quad (5.4.22)$$

where $PST_{b,T}$ is the position shift in centroid calculation due to asymmetrical positioning of the along-track reticle over the bands. $PST_{b,T}$ is 4.625 for 0.25 km IFOV bands, 4.75 for 0.5 km IFOV bands, 5 for 1 km IFOV bands.

5.4.7. Calculate the MODIS band centroid position shift along-track

$$\langle \Delta Y \rangle_b = \frac{1}{2} \sum_{side=1}^{2} \left[\langle Y \rangle_{b,side} - \langle Y \rangle_{b,side,prelaunch} \right] \quad (5.4.23)$$

The centroid position shift along-track is in the same direction as along-track. $\langle \Delta Y \rangle_b$ is plus if the band is shifted along-track. The reason is that the signal for the detector with higher Y value will be enhanced in result of higher $\langle Y \rangle_{b,side}$ when the detectors of a band is shifted along-track.

5.4.8. Calculate the current band centroid position along-track

$$\langle Y \rangle_{b,current} = \frac{1}{2} \sum_{side=1}^{2} \left[\langle Y \rangle_{b,side} + \langle \Delta Y \rangle_{b,side,o} \right] \quad (5.4.24)$$

where $\langle \Delta Y \rangle_{b,side,o} = \langle Y \rangle_{b,GSE} - \langle Y \rangle_{b,side,prelaunch}$ and $\langle Y \rangle_{b,GSE}$ is computed using GSE measured detector position along-track.

5.5. Mathematical description of the algorithm for determining the position shifts of the four FPAs

The four FPA shifts include FPA shift along-scan, FPA shift along-track, and FPA rotation.
When the detector/band positions for several bands are not available due to noisy or saturated detectors, their positions can be interpolated between known vicinity detector/band positions. In case detectors/bands are still noisy or located on the edge of the FPA, the FPA shift information can provide data to infer their positions.

According to the calibration results from the along-scan and along-track described in 5.3 and 5.4, the position shifts of the four FPA can be calculated (see Figure 5.5.1):

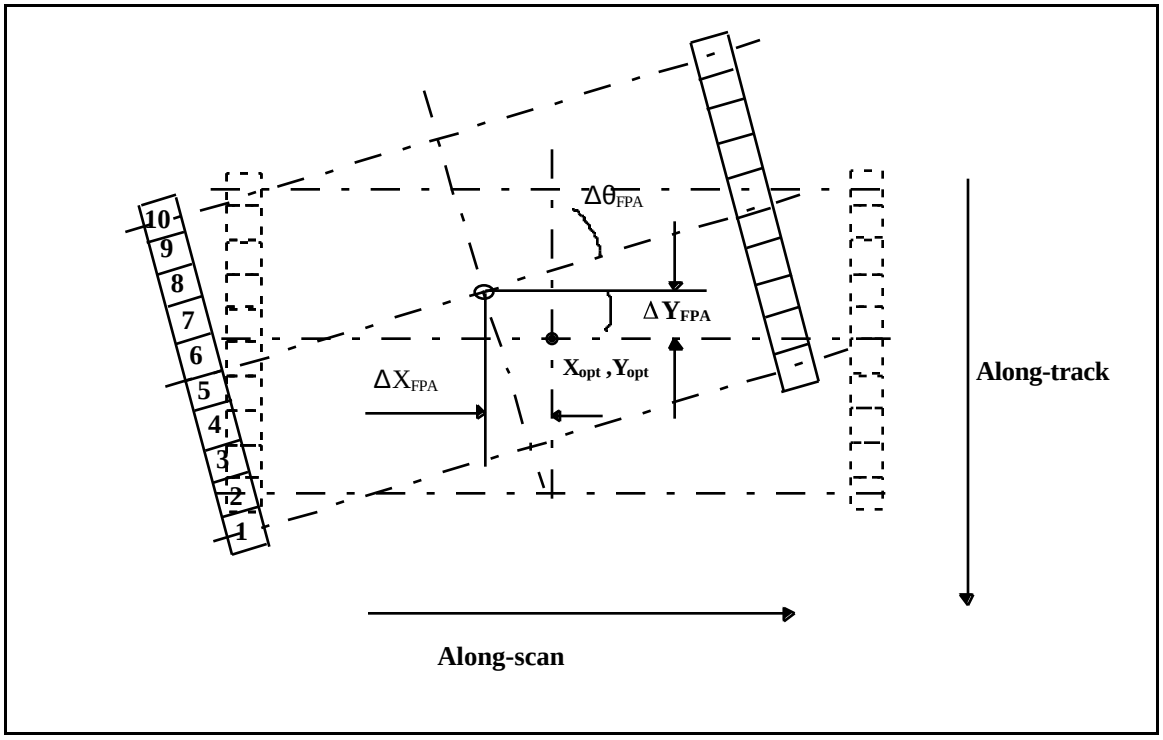

Figure 5.5.1 Geometry of the focal plane shifts

5.5.1 FPA rotation

The inclination of the detector-array of a band can be determined based on the knowledge of detector shift along-scan. The inclination angle for a band is calculated by the linear regression of the two data sets, $\langle X \rangle_{b,ch}$ and $Y_{b,ch,o}$, where subscription of 'o' indicates preluanch value. The change of current inclination angle from the prelaunch value is the detector-array rotation. Counting only for those bands in FPA rotation calculation if the active detector number in a band is greater than 70%, the average rotation angle of the detector-array for all bands in each individual FPA is

$$\Delta\theta_{FPA}(I) = \frac{1}{N_b(I)} \sum_{b=1}^{N_b(I)} \left[\theta_{LG}(Y_{b,ch,o}; \langle X \rangle_{b,ch}; b) - \theta_{LG}(Y_{b,ch,o}; \langle X \rangle_{b,ch,o}; b) \right] \quad (5.5.1)$$

where b is the band number, I is the FPA number, N_b is the number of bands in a FPA, θ_{LG} is the inclination angle.

The positive rotation is that the FPA rotates count-clockwise in X-Y coordinates as shown in Figure 5.5.1.

The magnification change would affect the actual $Y_{b,ch}$ from $Y_{b,ch,o}$ values applied in the formula, this effect causes a secondary error.

5.5.2 FPA magnification change

The magnification change could be caused by changes in the optical chain for each FPA. The optical chain is from the SRCA collimator to MODIS. It has different meaning from the magnification of MODIS because it does include the portion of the SRCA collimator. When magnification changes, the projected image sizes of the SRCA along-scan and along-track reticles will change. In along-scan, the width of the CARFS curve varies with the size of the along-scan reticle. For example, the CARFS curve will be widened if the magnification value increases. This provides a method to determine the magnification on-orbit.

$$\Delta M_{FPA}(I) = \frac{1}{N_b(I)} \sum_{b=1}^{N_b(I)} \frac{1}{N_{ch}(b)} \left[\sum_{ch=1}^{N_{ch}(b)} \frac{\langle X_{half,r} \rangle_{b,ch} - \langle X_{half,l} \rangle_{b,ch}}{\langle X_{half,r} \rangle_{b,ch,o} - \langle X_{half,l} \rangle_{b,ch,o}} \right] - 1 \qquad (5.5.2)$$

where $\langle X_{half,r} \rangle$ *and* $\langle X_{half,l} \rangle$ are the right and left X values corresponding to half maximum response of the CARFS on both sides. The subscript 'o' stands for prelaunch value.

5.5.3 FPA shift along-scan

The FPA shift along-scan is the average shift along-scan for all detectors in a FPA. All active detectors are counted in the calculation.

$$\Delta X_{FPA}(I) = \frac{1}{N_b(I) N_{ch}(b)} \sum_{b=1}^{N_b(I)} \left[\sum_{ch=1}^{N_{ch}(b)} (\langle X \rangle_{b,ch} - \langle X \rangle_{b,ch,o}) \right] \qquad (5.5.3)$$

where ***ch*** is the channel number, N_{ch} is the number of channel for a band, The rest of notation is the same as section 5.5.1.

5.5.4 FPA shift along-track

FPA rotation needs to be considered in the calculation of FPA shift along-track because rotation causes the centroid position to shift along-track. The compensation value is related to the distance from the optical center to the band position along-scan and the rotation angle.

The magnification change will bias the centroid Y values because of asymmetric placing of the along-track reticle over the detectors for a band. Figure 5.5.2 shows the centroid Y changes with magnification. The curves are determined when the detectors are located at

ideal position with ideal size and no gaps between detectors. After the magnification on-orbit has been calculated, the corrected centroid Y for the Ith FPA , $\langle \Delta Y \rangle_{mag}(I)$, can be calculated by interpolation. The data base for $\langle \Delta Y \rangle_{mag}(I)$ will be given after the detector positions at the FPA are measured by GSE.

The FPA shift along-track can be written as

$$\Delta Y_{FPA}(I) = \frac{1}{N_b(I)} \sum_{b=1}^{N_b(I)} \left[\langle Y \rangle_b - \langle Y \rangle_{b,o} - \frac{\sin(\Delta\theta_{FPA}(I))}{N_{ch}} \left(\sum_{ch=1}^{N_{ch}(b)} (\langle X \rangle_{b,ch,o} - \langle X \rangle_{opt}(I)) \right) \right] - \Delta \langle Y_{mag}(I) \rangle \tag{5.5.4}$$

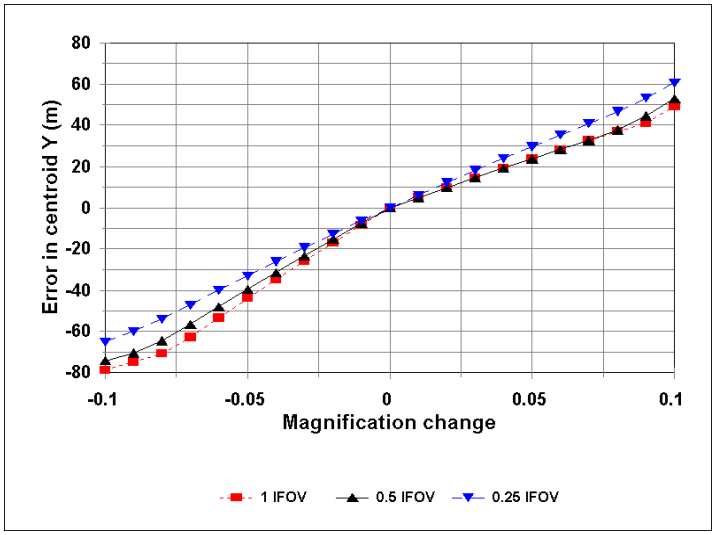

where $\langle Y \rangle_b$ and $\langle Y \rangle_{b,o}$ are the centroid value of a band along-track measured on-orbit and prelaunch. $\langle X \rangle_{opt}$ is the $\langle X \rangle$ value of the optical axis for each FPA measured prelaunch as data base value. ΔY_{MAG} is the compesation item due to magnification change.

Figure 5.5.2 $\langle \Delta Y \rangle_{mag}$ as a function of magnification change

5.6 Strategy for determining detector position along scan and band centroid position along track for various levels of signal quality

Table 5.6.1 and 5.6.2 present strategies for determining detector position along-scan and along-track, respectively.

Table 5.6.1 Strategy for determining position along scan

Band/detectors quality of signal	Detector along scan
All detector in the band have adequate signal	Section 5.3
Up to 30% the detectors have inadequate signal in a band	Section 5.3 for detectors with adequate signal Section 5.7, case 3 for detectors with inadequate signal
A band with inadequate signal sandwiched between two bands with adequate signal	Section 5.7, case 1
A band with inadequate signal at an edge of the FPA	Section 5.7, case 2

Table 5.6.2 Strategy for determining centroid position along track

Band/detectors quality of signal	Band centroid along track
All detector in the band have adequate signal	Section 5.4
Any detector in band has inadequate signal	Section 5.7, case 2

Section 5.3 presents an algorithm for determining detector positions along scan for any detector with an adequate signal. A detector has an adequate signal if it has a good signal to noise ratio and it is not saturated. If every detector in a band has an adequate signal then the algorithms presented in Section 5.4 may be used to determine the centroid of the whole band along track; conversely, if even one detector in the band has inadequate signal then the algorithms can not be used. For bands containing detectors with inadequate signals, Section 5.7 presents algorithms for determining detector positions along scan and band centroid position along track.

5.7 Description of the algorithm of determining the detector position and its shift for noisy/saturated channels/bands (Figure 5.7.1)

Case 1. The noisy/saturated band is sandwiched between other bands.

Assume that the noisy/saturated band is ***bx*** . Let the band next to it but with smaller data frame number be ***blf*** and the band next to it but with greater data frame number be ***brt***. The prelaunch measured distances along-scan, subscripted by ***o,*** are

$$S_{lf} = \left| \langle X \rangle_{bx,ch,o} - \langle X \rangle_{blf,ch,o} \right| \text{ and } S_{rt} = \left| \langle X \rangle_{brt,ch,o} - \langle X \rangle_{bx,ch,o} \right| \qquad (5.7.1)$$

The shifts of band ***bx*** are

$$\langle \Delta X \rangle_{bx,ch} = \frac{S_{lf}}{S_{lf} + S_{rt}} \left[\langle \Delta X \rangle_{brt,ch} - \langle \Delta X \rangle_{blf,ch} \right] + \langle \Delta X \rangle_{blf,ch} \quad (5.7.2)$$

$$\langle \Delta Y \rangle_{bx} = \frac{S_{lf}}{S_{lf} + S_{rt}} \left[\langle \Delta Y \rangle_{brt} - \langle \Delta Y \rangle_{blf} \right] + \langle \Delta Y \rangle_{blf} \quad (5.7.3)$$

The calculation is valid only if the number of detectors for band ***bx*** is equal or less than both bands, ***blf*** and ***brt***. Conversely, the method introduced in case 2 is applied.

Case 2. The noisy/saturated band is the leftmost or the rightmost band in the FPA

In this case, we need to use FPA shift information to determine the band/detector shifts. The distances between the detector center and the optical center measured prelaunch are

$$S_{bx,ch,x} = \left| \langle X \rangle_{bx,ch,o} - \langle X \rangle_{opt,o} \right| \quad \text{and} \quad S_{bx,ch,y} = \left| Y_{bx,ch,o} - Y_{opt,o} \right| \quad (5.7.4)$$

The distance between the detector center and the optical center measured prelaunch is

$$D_{b,ch} = (1 + \Delta M_{FPA}(I)) \cdot \sqrt{S_{bx,ch,x}^2 + S_{bx,ch,y}^2} \quad (5.7.5)$$

and $\sin\theta_{b,ch} = S_{bx,ch,y} / D_{b,ch}$, $\cos\theta_{b,ch} = S_{bx,ch,x} / D_{b,ch}$

The detector shift along-scan

$$\langle \Delta X \rangle_{bx,ch} = (1 + \Delta M_{FPA}(I)) \cdot \left[S_{bx,ch,x} \cdot (\cos(\Delta\theta_{FPA}(I)) - 1) - S_{bx,ch,y} \cdot \sin(\Delta\theta_{FPA}(I)) \right] + \langle \Delta X \rangle_{FPA}(I) \quad (5.7.6)$$

The band centroid shift along-track

$$\langle \Delta Y \rangle_{bx} = \frac{\sin(\Delta\theta_{FPA}(I))}{N_{ch}} \cdot \sum_{ch=1}^{N_{ch}} S_{bx,ch,x} + \langle \Delta Y \rangle_{FPA}(I) \quad (5.7.7)$$

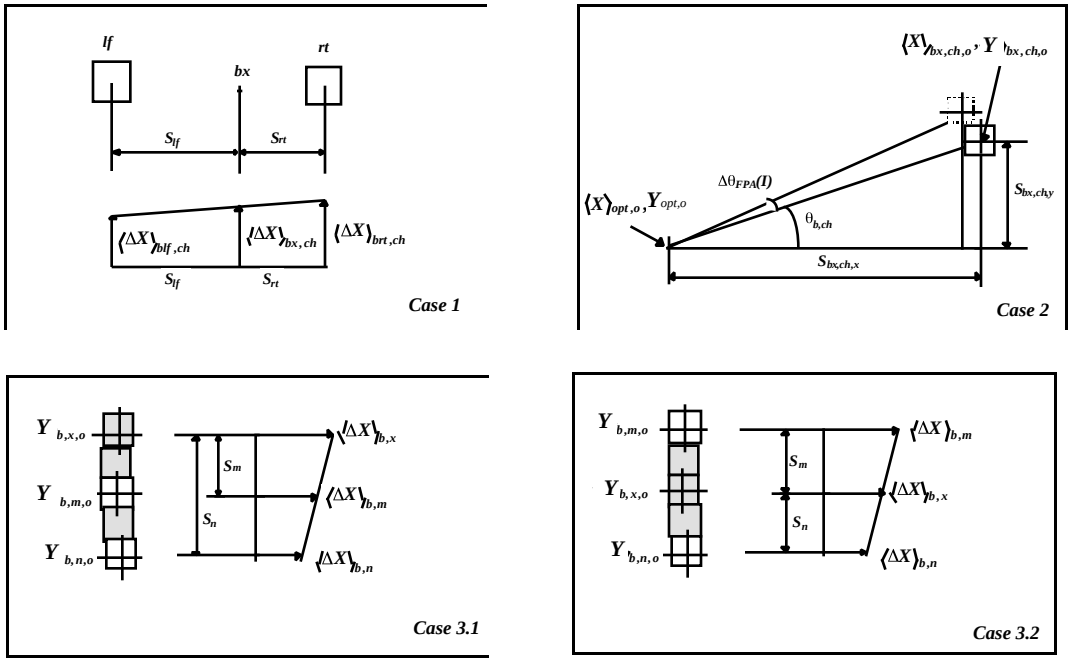

Figure 5.6.1 Determination of shift along-scan for noisy/saturated detector

Case 3. If the band ***blf*** or/and band ***brt*** contains noisy/saturated detector

The detector shift on-orbit is calculated by interpolation or extrapolation of their neighbor detectors. In the Figure 5.7.1 the shaded detectors are assumed as noisy/saturated detectors.

Case 3.1 The noisy/saturated detector, ***x***, is located on the both ends of a band. The detector shift along-scan is extrapolated from two of nearest active detectors, ***m*** and ***n***, of a band.

$$S_m = \left| Y_{b,m,o} - Y_{b,x,o} \right| \text{ and } S_n = \left| Y_{b,n,o} - Y_{b,x,o} \right| \tag{5.7.8}$$

$$\langle \Delta X \rangle_{b,x} = \langle \Delta X \rangle_{b,n} + \left[\langle \Delta X \rangle_{b,m} - \langle \Delta X \rangle_{b,n} \right] \cdot \left(\frac{S_n}{S_n - S_m} \right) \tag{5.7.9}$$

The centroid shift along-track uses Eq.(5.7.7).

Case 3.2 The noisy/saturated detector is sandwiched. The detector shift along-scan is interpolated from two of nearest active detectors, ***m*** and ***n***, of a band.

$$\langle \Delta X \rangle_{b,x} = \langle \Delta X \rangle_{b,n} + \left[\langle \Delta X \rangle_{b,m} - \langle \Delta X \rangle_{b,n} \right] \cdot \left(\frac{S_n}{S_m + S_n} \right) \qquad (5.7.10)$$

The centroid band shift along-track uses Eq.(5.7.7)

5.8 Uncertainty estimates

Table 5.8.1 Uncertainty budget for the SRCA spatial calibration (at 1 σ confidence level)

Item	Description of uncertainty sources	Uncertainty	Band 8 case (m)
1	Lamp output variation and drift	0.25%	negligible
2	SNR and quantization	1/DN/√No. averaged	negligible
3	Non-uniform illumination along-track	Simplified STOP	2
4	Non-uniform illumination along-scan	Simplified STOP	2
5	Phase-delay variation	0.01 IFOV	2
6	Partial aperture filling		N/A
7	Defocus	0.5 mm	negligible
8	Cross-talk	4% distributed to neighbor detector	9
9	FPA/Reticle imaging inclination by 3 arc sec.; shift along-scan/along-track of 0.1 IFOV(1 km); and magnification change by 5%	Along-scan	4
		Along-track	15
Total (Inter-FPA case)			18

Table 5.8.1 lists the uncertainty budget for the SRCA spatial calibration. When the SRCA reticle or the MODIS optical chain, shared by the four FPA, are shifted, no error is introduced for the relative co-registration of the detectors. However, the shifts for the individual optical chain for each FPA affect the relative co-registration. Summary of these uncertainties is shown in Table 5.8.1. Table 5.8.2 is the uncertainty requirement for relative co-registration. The requirement is 0.2 IFOV and the goal is 0.1 IFOV.

Table 5.8.2 The uncertainty budget of relative co-registration (m)

(at 1σ confidence level)

	1km - 1km	0.5km - 0.5km	0.25km - 0.25km	1km - 0.5km	1km - 0.25km
Specification	200	100	50	200	200
Goal	100	50	25	100	100

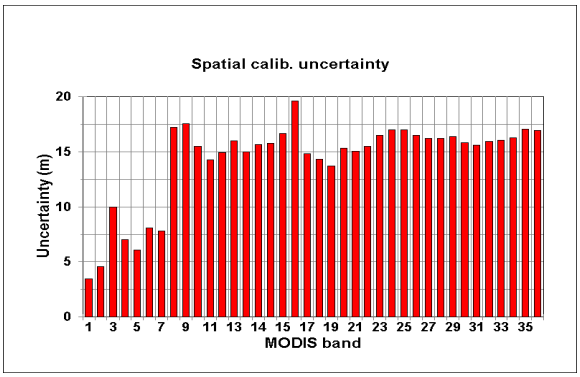

Figure 5.8.1 Uncertainty estimate

Table 5.8.3 Relative shift and geolocation uncertainties (m)

(at 1 σ confidence level)

	1km - 1km	0.5km - 0.5km	0.25km - 0.25km	1km - 0.5km	1km - 0.25km
1. Relative shift					
Prelaunch (1)	35	18	9	28	26
SRCA on-orbit	24	13	6	19	18
Total	42	22	12	34	32
2. Geolocation					
After A&E SDST provides (2)	19	19	19	19	19
Total	46	29	22	39	37

1) Prelaunch data is calculated by ground measurement with a resolution of 1/40 IFOV (SBRC)

2) SDST provides geolocation of 10 nominal 1-km IFOVs in a single band with a location uncertainty (3σ) :97m along-scan, 75m along-track (at launch) and 51m along-scan, 28m along-track (after A & E).

The uncertainties for all bands from Table 5.8.1 are evaluated from Monte-Carlo simulation and the result is shown in Figure 5.8.1. For comparison with the specification on the band relative co-registration, the square-root of the two individual band values gives the relative band position shift. The average uncertainty of the relative shift for different detector size combination is given in Table 5.8.3. In combination with the detector position measurement uncertainty prelaunch and the geolocation for a nominal band, the on-orbit geolocation uncertainty is calculated. More pertain analysis will be given after the measurement data in the laboratory or in TV are available.

5.9 Description of input data set, output products, and quality control

5.9.1 Input data set:

1) Detector relative position, $\langle X \rangle_{b,ch,o}$ and $Y_{b,ch,o}$, for all bands measured by the GSE prelaunch at TV.

2) Correction coefficients considering the SRCA partial aperture illumination for each detector along-scan, $\langle \Delta X \rangle_{b,ch,o}$,and each band along-track, $\langle Y \rangle_{b,o}$.

3) Optical axis position for each FPA, $\langle X \rangle_{opt}(I)$.

5.9.2 Output products

1) Detector position shift along-scan, $\langle \Delta X \rangle_{b,ch}$,and centroid position shift along-track, $\langle \Delta Y \rangle_{b}$.

2) Detector position along-scan, $\langle X \rangle_{b,ch}$,and centroid position along-track, $\langle Y \rangle_{b}$.

3) Off-line products: Four FPA relative shifts along-scan, $\Delta X_{FPA}(I)$, along-track, $\Delta Y_{FPA}(I)$, and rotation, $\Delta\theta_{FPA}(I)$, and magnification change, $\Delta M_{FPA}(I)$.

5.9.3 Quality control and exception handling

1) The signals for MODIS detectors are averaged over multi-scan. Standard deviations are calculated as criteria to set instability flags.

2) The position shift along-scan will be evaluated by interpolation from the detector positions of their vicinity bands or by using FPA shift information if the band/channel is saturated or noisy.

3) The centroid position and its shift along-track is determined for the band if one of the active channel signal is noisy/saturated.

4) A band will be excluded from the FPA position shift calculation if less than 70% detector is active for that band.

5) See 3.4.4 (2).

6) FPA shift malfunction flags: shift along-scan > 0.4 IFOV, shift along-track > 0.4 IFOV, rotation > 2°, and magnification change > 5%. (to be modified after ground measurement data available)

References

[1] "Operational in-flight calibration procedures (Preliminary report)", CDRL 404, SBRC.
[2] "Spectral band registration (SBR) conceptual measurement methodology", SBRS Internal Memorandum, PL3095-N01338, by J. Young, July 1992.
[3] "Ambient calibration and testing (AC) support software, requirements for", A11323-151868, SBRS, 1993.
[4] "Critical design review for the Moderate Resolution Imaging spectroradiometer (MODIS)", SBRS, Jan. 1994.
[5] "SRCA along track SBR modeling/algorithm ", SBRS Internal Memorandum, PL3095-N04214, by J. young, Aug. 1994.
[6] "ATBD for MODIS level 1B algorithm", MODIS algorithm team (MAT), Dec. 1994.
[7] "Software Requirements Specification for the MODIS Level 1B Software System", P200-CD-001-001, MODIS Characterization Support Team, June 15, 1995.
[8] "MODIS operations concept document [M0007]", by K. Parker and Ed. Knight, Nov. 1995.
[9] "MODIS level 1B Algorithm Theoretical Document 1995 [MOD-02]", B.M. Jones, H. Montgomery, R. Veiga, D. Knowles Jr., N. Che, L. Goldberg, Dec. 1995.
[10] "Response to SRCA questions from GSFC", SBRS Internal Memorandum, PL3095-Q06002, by E. Johnson, Aug. 1996.

6. Notation

A	Grating spacing
A_{ND}	Adjustment coefficient for determining the transmittance of the neutral density filter
$A(\lambda)$	A spectral configuration factor which accounts for the difference in the spectral profile between the blackbody and the SRCA. This factor mainly includes the spectral profile of the SRCA source output, the spectral reflectance of the SRCA integration sphere wall material, and the SRCA transmittance.
A_{Ω}	Effective solid angle-area product of lamp filament
$ARFS$	Aperture Response Function along-Scan
ART	Aperture Response along-Track
b	Band number
blf	The band which is located next to the noisy/saturated band with a smaller data frame number
b_o	The reference band number
brt	The band which is located next to the noisy/saturated band with a greater data frame number
$c(b\#)$	A coefficient which compensates for the difference in the spectral profiles between two operational lamp radiometric temperatures
$C_{SRCA}(b,ch)$	Correction coefficient of non-uniform output of the SRCA
$CARFS$	Combined Aperture Response Function along-Scan
$CDS_{AV,L}(\theta_m,m)$	The average value of the $CDS_L(\theta_m,m)$
$CDS_L(\theta_m,m)$	The DN value of the calibration SiPD for lamp configuration, L, grating angle, θ_m, and diffraction order, m

$CDS_{norm,L}(\theta_m,m)$ The ***$CDS_L(\theta_m,m)$*** normalized by the ***$SDS_L(\theta_m,m)$***

ch Channel number

DN_{AV} Average ***DN*** value

$DN_{b,ch,L}$, $DN_{b,ch,R}$ The averaged DN corresponding to the left/right openings for along-track reticle.

DN_{max} The maximum ***DN***

$DN_{ref}(\lambda)$ ***DN*** value of the reference SiPD at wavelength of λ

$DN_{SIS}(lamp,sample)$ MODIS detector ***DN*** value under SIS(100) illumination for lamp configuration, ***lamp,*** and sample number, ***sample***

DN_{SRCA} MODIS detector ***DN*** value under the SRCA illumination

$DN_{threshold}$ Threshold of digital counts

$E_{SIS}(\lambda)$ Efficiency of the SRCA SIS

F_{lf} Left frame number

F_{rt} Right frame number

F_{mid} Middle frame number

$F(\lambda)$ Relative profile of the radiant flux

Frame# Frame number

G(b#) Radiometric gain value for band *b#*

IFOV Instantaneous field of view

Integer[ ] Take integer for the result in ***[ ]***

$l_{slit}(\lambda)$ Relative profile measured at the exit slit plane

$l_{SRCA}(\lambda)$ The relative spectral profile of the SRCA

$L_b(\lambda,T)$ The spectral radiance of the blackbody at wavelength λ and temperature of T

$L_{SIS(100)}(lamp, \lambda)$ The spectral radiance of the SIS(100) for the lamp configuration of "lamp"

$L_{SRCA}(b\#)$ Effective in-band radiance of the SRCA

$L_{SRCA}(\lambda)$ Effective spectral radiance of the SRCA

m Diffraction order

$M_{FPA}(I)$ Magnification of the focal plane I

$MSR(b\#,ch\#,\lambda)$ The MODIS detector signal in terms of wavelength. This signal has been normalized by the spectral profile of the SRCA SIS source

$MSR_L(b\#,ch\#,\theta_m,m)$ The MODIS detector ***DN*** value for band, ***b#,*** channel, ***ch#,*** grating angle, θ_m, and diffraction order, ***m***.

$MSR_{norm,L}(b\#,ch\#,\theta_m,m)$ $MSR_L(b\#,ch\#,\theta_m,m)$ normalized by the reference detector response

$N_b(I)$ Number of bands in focal plane ***I***

N_{ch} Number of channels in a band

$N_{ch}(b)$ Number of channels for band ***b***

N_{frame} Number of frames

N_{phase} Number of phase-delays

N_{side} Number of scan mirror sides, equal to two

N_{scan} Number of scans

Phase#Phase-delay number

Phase-length	The spatial difference between two continuous phase-delay settings
$PST_{b,S}$, $PST_{b,T}$	The position shifts in centroid calculation along-scan/along-track
q_{coef}	A constant to average out the signal level in Least-square fitting
$R(b\#,\lambda)$	The spectral response of the MODIS band ***b#*** measured prelaunch in TV
$R_{CDS}(\lambda)$	The spectral response of the calibration SiPD
$R_{SDS}(\lambda)$	The spectral response of the reference SiPD
$\Delta R(\lambda,T)$	The spectral temperature coefficient of the reference SiPD under the operational temperature of "T"
Scan#	Scan number
$SDS_L(\theta_m,m)$	The same as $CDS_L(\theta_m,m)$ but for the reference SiPD
$SDS_{AV,L}(\theta_m,m)$	The average value of the $SDS_L(\theta_m,m)$
Side#	Scan mirror side number
step	The grating motor step number
std[ ]	Calculation of standard deviation
U(b,ch)	Gain inconsistency between channels
X_b	Position of a band center along the focal plane assembly
$\langle X \rangle_{b,ch}$	The spatial center position for a detector along-scan
$\langle X \rangle_{b,ch,o}$	The spatial center position for a detector measured prelaunch along-scan
$\langle X \rangle_{opt}(I)$	The optical axis position along-scan for focal plane ***I***

$<\Delta X>_{b,ch}$	Detector position shift along-scan on-orbit
$<\Delta X>_{b,ch,o}$	Detector position difference measured by the GSE and the SRCA due to the SRCA partial aperture filling
$\Delta X_{FPA}(I)$	Focal plane shift on-orbit along-scan
$Y_{b,ch}$	The weighted coordinate of a detector along-track
$Y_{b,ch,o}$	The detector center position measured prelaunch by the GSE along-track
$<Y>_b$	The centroid band position on-orbit along-track
$<Y>_{b,o}$	The centroid band position measured prelaunch along-track
$\Delta Y_{FPA}(I)$	Focal plane shift on-orbit along-track
$<\Delta Y>_b$	The centroid position shift along-track
$<\Delta Y>_{b,o}$	The centroid position difference between the spatial position calculated from the measurement data by the GSE and measured by the SRCA
β	Half of the angle between the incident ray and the exit ray relative to the grating
β_o	Nominal β value
$\varepsilon(\lambda)$	Lamp filament emissivity
Δ	The angular displacement between the main exit slit and the didymium slit
θ_{LG}	Angle calculated by the linear regression
θ_m	Grating angle
$\theta_{m,pk}$	Grating angle at didymium peak region

$\theta'_{m,pk}$	Grating angle for the reference SiPD, which equals to the $\theta_{m,pk}$ after a physical shift required to match $\theta_{m,pk}$ at didymium peak region
θ_{off}	The offset angle of the grating motor
θ_{offo}	Nominal θ_{off} value
$\Delta\theta_{FPA}$	The focal plane rotation on-orbit
λ_c***(b#,ch#)***	The center wavelength value for band ***b#*** and channel ***ch#***
$\lambda_{cut\text{-}in}$	Cut-in wavelength corresponding to half of the maximum band response
$\lambda_{cut\text{-}off}$	Cut-out wavelength corresponding to half of the maximum band response
$\lambda_{pk}^{didymium}$	The wavelength value of the didymium glass at the peak number of "pk"
$\lambda_{pk,L}^{dCDS}$	Wavelength corresponding to the centroid step motor angle of the transmission peak
$\Delta\lambda_c$	The center wavelength shift
$\Delta\lambda_o$	Center wavelength correction value for the measurement difference between GSE and the SRCA prelaunch in TV
$\Delta\lambda$***(b#,ch#)***	The bandwidth for band ***b#*** and channel ***ch#***
$\tau_{didymium}(\lambda)$	The transmittance of the didymium absorption glass
$\tau_{ND}(\lambda)$	The spectral transmittance of the neutral density filter
τ_{ND}***(b#)***	The in-band transmittance of the neutral density filter
$\Omega_{m,pk,L}^{CDS}$	The centroid grating angle for the peak number of "pk", calculated from calibration SiPD signal

.

7. Acronyms

A&E	Activation and Evaluation
BB	Blackbody
DN	Digital counts
EOS	Earth Observing System
Eq.	Equation
FPA	Focal plane assembly
GSE	Ground support equipment
GSFC	Goddard Space Flight Center
IFOV	Instantaneous field of view
IR	Infrared
LWIR	Long wave infrared
MCST	MODIS Characterization Support Team
MODIS	Moderate Resolution Imaging Spectroradiometer
MWIR	Middle wave infrared
ND	Neutral density
NIR	Near infrared
NIST	National Institute of Standard Technology
OBC	Onboard calibrator
SBRS	Hughes Santa Barbara Remote Sensing (original Santa Barbara Research Center (SBRC))
SD/SDSM	Solar Diffuser/Solar Diffuser Stability Monitor
SDST	Science Data Support Team
SNR	Signal to noise ratio
SiPD	Silicon Photodiode
SIS	Spherical integrating source
SIS(100)	SIS of 100 cm in diameter, a ground radiometric calibration source
SRCA	Spectro-Radiometric Calibration Assembly
SWIR	Short wave infrared
TBD	To be determined
TV	Thermal vacuum testing
VIS	Visible

Appendix A. Determination of the SRCA spectral radiance prelaunch

The SRCA is calibrated against the SIS(100) at TV. During the calibration MODIS will be alternately illuminated by the SIS(100) and the SRCA. The in-band radiance of the SIS(100) is known. After subtracting the space view signal counts and correcting for the MODIS detector non-linearity, scan mirror reflectivity, temperature-related DN change, and scan angle effect, the corrected DN values are available. The effective in-band radiance is

$$L_{SRCA}(b\#,ch\#) = L_{SIS(100)}(b\#,ch\#) \bullet \frac{DN_{SRCA}(b\#,ch\#)}{DN_{SIS(100)}(b\#,ch\#)} \qquad \text{(A.1)}$$

The "effective" is in the sense that the SRCA output radiance, partially fills the MODIS aperture, produces the same $DN_{SRCA}(b\#,ch\#)$ value as an extended radiance source, with radiance of $L_{SRCA}(b\#,ch\#)$, at the MODIS entrance pupil. For simplicity, we call the SRCA effective radiance as SRCA radiance in this document.

Conversion of the SRCA in-band radiance to spectral radiance is needed for determining the spectral radiance change on-orbit. When the spectral radiance of a source is slowly varying and the bandwidth is narrow, the spectral radiance at the center wavelength is approximated by

$$L_{SRCA}(\lambda_c) = \frac{\frac{1}{N_{ch}(b\#)} \sum_{1}^{N_{ch}(b\#)} L_{SRCA}(b\#,ch\#)}{\Delta\lambda(b\#)} \qquad \text{(A.2)}$$

where the center wavelength for band b# [1] is

$$\lambda_c = \int_0^\infty \lambda R(\lambda)\, d\lambda \Big/ \int_0^\infty R(\lambda)\, d\lambda \qquad \text{(A.3)}$$

the bandwidth [1] is

$$\Delta\lambda = \lambda_2 - \lambda_1 = \sqrt{12(M - \lambda_c^2)} \qquad \text{(A.4)}$$

R(λ) is the spectral response of the band and

$$M = \int_0^\infty \lambda^2 R(\lambda)\, d\lambda \Big/ \int_0^\infty R(\lambda)\, d\lambda \qquad \text{(A.5)}$$

A modeling curve fits the available SRCA spectral radiances $L_{SRCA}(\lambda_c)$.

$$L_{SRCA}(\lambda, T) = q_{coef} \cdot A(\lambda) \cdot L_b(\lambda, T) \quad \text{(A.6)}$$

where the $A(\lambda)$ is determined using the SRCA relative output profile by

$$A(\lambda) = \frac{l_{SRCA}(\lambda)}{L_b(\lambda, T_o)} \quad \text{(A.7)}$$

The $A(\lambda)$ is the combination of the SRCA transmittance, the SRCA SIS efficiency, lamp filament emissivity, and other spectral modification such as mirror reflectivity. It is assumed that $A(\lambda)$ does not change during A&E. In Eq. (A.7) T_o is the radiometric temperature measured when the SRCA relative output profile measures.

A least-square fit method [3] is utilized to fit the model to the known $L_{SRCA}(\lambda_c)$ until a T and q_{coef} values are obtained.

The first derivatives of $L_{SRCA}(\lambda_i, T)$ with respect to q_{coef} and T on-orbit are

$$ds_{coef,i} = \frac{\partial L_{SRCA}(\lambda_i, T)}{\partial q_{coef}} = A(\lambda_i) \cdot L_b(\lambda_i, T) \quad \text{(A.8)}$$

and

$$ds_{T,i} = \frac{\partial L_{SRCA}(\lambda_i, T)}{\partial T} = q_{coef} \cdot \frac{14388}{\lambda_i T^2} \cdot A(\lambda_i) \cdot L_b(\lambda_i, T) \quad \text{(A.9)}$$

The difference is between fitting curve and the known SRCA spectral radiance at the center wavelength for data point i is

$$R_{ss,i} = q_{coef} \cdot A(\lambda_{c,i}) \cdot L_b(\lambda_{c,i}, T) - L_{SRCA}(\lambda_{c,i}) \quad \text{(A.10)}$$

where λ_i is selected to equal $\lambda_{c,i}$ in Eqs. (A.8), A(9), and (A.10).

The matrix coefficients are:

$$C_{11} = \sum_{i=1}^{N} ds_{coef,i}^2 \quad \text{(A.11)}$$

$$C_{12} = C_{21} = \sum_{i=1}^{N} ds_{coef,i} ds_{T,i} \quad \text{(A.12)}$$

$$C_{22} = \sum_{i=1}^{N} ds_{T,i}^2 \tag{A.13}$$

$$D_{coef} = \sum_{i=1}^{N} R_{ss,i} \cdot ds_{coef,i} \tag{A.14}$$

$$D_T = \sum_{i=1}^{N} R_{ss,i} \cdot ds_{T,i} \tag{A.15}$$

Least-square fit method [3]:

(1) Start with an initial temperature, T_{ini}
(2) Calculate call matrix coefficients.
(3) Solve the matrix

$$\begin{bmatrix} \Delta_{coef} \\ \Delta_T \end{bmatrix} = \begin{bmatrix} C_{11} & C_{12} \\ C_{21} & C_{22} \end{bmatrix}^{-1} \cdot \begin{bmatrix} D_{coef} \\ D_T \end{bmatrix} \tag{A.16}$$

(4) The current $q_{coef} = q_{coef} - \Delta_{coef}$ and $T_{on-orbit} = T_{on-orbit} - \Delta_T$ (A.17)

(5) Iterate (back to step (2)) until q_{coef} and $T_{on\text{-}orbit}$ are converged.

Finally, the SRCA spectral radiance is given by Eq. (A.10). This procedure must be done for lamp configurations of 3-10W and 1-10W).

References

[1] "Broadband radiometry with spectrally selective detectors", Optical Letter, 5(5):208-210, by J.M. Palmer and M.G. Tomasko, 1980.
[2] "Spherical Integrator Source, SIS(100) radiometric model simulation", SBRS Internal Memorandum, PL3095-N04231, by J. Young, Sep. 1994.

[3] "Polarized Source Assembly (PSA) simulation modeling", SBRS Internal Memorandum, PL3095-N04230, by J. Young, Sep. 1994.

[4] "SRCA radiometric calibration algorithm",SBRS Internal Memorandum, PL3095-Q05746, by R. Osgood, May 3, 1996.

Appendix B. Methodology of deduction of lamp temperatures based upon measured spectral profile at the exit slit plane of the SRCA

The spectral output will be measured at the exit slit plane of the SRCA at subassembly level.

1. Deduction of the spectral profile of the SRCA.

Knowing the spectral reflectivity of mirror coating, $\rho_{mirror}(\lambda)$, for the telescope and the plain mirror in front of the exit plane, the spectral profile of the SRCA output is

$$I_{SRCA}(\lambda) = I_{slit}(\lambda) \cdot (\rho_{mirror}(\lambda))^4 \quad \text{(B.1)}$$

where $I_{SRCA}(\lambda)$ is the relative spectral profile measured at the exit slit plane by SBRS.

2. Deduction of lamp temperature of the SRCA SIS lamp.

The method is to use a set of models which has been examined in the Lab. to determine the spectral profile of the lamp output. Then the radiometric temperature value is calculated by least-square fit.

The models to describe the lamp emissivity, SIS efficiency, and blackbody radiance are

Lamp emissivity, $\varepsilon(\lambda,T)$, is [1]

$$\varepsilon(\lambda,T) = (0.7641 - 0.0000875T) \cdot \exp(-(0.759 - 0.0001488T) \cdot \lambda) \quad \text{(B.2)}$$

The efficiency of the SRCA SIS, $E_{SIS}(\lambda)$, is [1]

$$E_{SIS}(\lambda) = \frac{A_e \cdot \rho_W(\lambda)}{(1 - \rho_W(\lambda)) \cdot A_W + \rho_W(\lambda) \cdot (A_e + A_i)} \quad \text{(B.3)}$$

where $\rho_W(\lambda)$ is the diffuse reflectance of the SIS wall material, A_W is the area of the coated wall, A_e is the area of SIS exit hole, A_i the area which includes the holes for lamps and SiPDs.

The blackbody radiance ($Wcm^{-2}sr^{-1}\mu m^{-1}$) uses Planck's equation, that is

$$L_b(\lambda,T) = \frac{37420}{\pi\lambda^5 \cdot \left[\exp\left(\frac{14388}{\lambda T}\right) - 1\right]} \quad \text{(B.4)}$$

The spectral transmittance of the SRCA, $\tau_{SRCA}(\lambda)$, is from the measurement by SBRS or from the calculation using CODE V.

The spectral profile of the SRCA at the exit slit plane can be expressed as

$$l_{SRCA}(\lambda, T) = K_{scale} \cdot \frac{A_{\Omega}}{\pi A_e} \varepsilon(\lambda, , T) \cdot L_b(\lambda, T) \cdot E_{SIS}(\lambda) \cdot \tau_{SRCA}(\lambda) \qquad \text{(B.5)}$$

where A_{Ω} is the effective solid angle-area product of lamp filament (cm^2sr).
Thus, the lamp radiant source as a blackbody emits the radiant flux with the spectral profile of

$$F(\lambda) = \frac{l_{Slit}(\lambda)}{\varepsilon(\lambda, T_o) \cdot E_{SIS}(\lambda) \cdot \tau_{SRCA}(\lambda)} \qquad \text{(B.6)}$$

where T_o uses the nominal temperature of the lamp filament.

This profile, $F(\lambda)$, is to fit the spectral radiant distribution curve of a blackbody at the temperture of T. The methodlogy is introduced in [2] and the algorithm can be refered to Appendix A.

References:

[1] “Modeling and testing of SRCA SIS radiant output”, SBRS Internal Memorandum, PL3095-Q03202, by E. Johnson, Oct 29, 1993.

[2] Optical radiation measurement, Vol. 1, by F. Grum and R.J. Becherer, Academic Press, 1979.